CALIFORNIA STATE UNIVERSITY, FRESNO

THE DIVISION OF GRADUATE STUDIES

THESIS OFFICE

The following template was developed for Department of Physics students using LaTeX to format their master's degree theses to conform to the publication requirements of the California State University, Fresno *Guidelines for Thesis Preparation*. Any use beyond the intended is prohibited without permission of the Division of Graduate Studies.

Note: The following "Final Draft Submission" approval page must be signed by all thesis committee members in order for the thesis to be reviewed in the graduate office.

Questions regarding formatting should be directed to:

Chuck Radke, Thesis Consultant

cradke@csufresno.edu

559-278-2418

ABSTRACT

THE 2012 OUTBURST OF THE SOFT X-RAY TRANSIENT/BLACK HOLE CANDIDATE SWIFT J1910.2-0546/MAXI J1910-057

We present optical differential photometry of the soft X-ray transient/black hole candidate Swift J1910.2-0546/MAXI J1910-057. The light curve exhibits aperiodic flickering behavior that appears to increase throughout our observations as well as the presence of several optical quasi-periodicities of 4.19 min and 13.08 min. After dividing the observations into five sections, we find only one quasi-periodicity of ∼11 cycles/day (2.17 h) that repeats in two of the five sections. A possible orbital period scenario was proposed where $P_{orb} = 2.17$ h. We calculated a period excess $\epsilon = 0.559$, which leads to a physically impossible mass ratio $q = 1.11$. Thus, we confidently conclude that no superhumps were detected in Swift J1910. With superhumps ruled out, the lone quasi-periodicity we detect is the most promising candidate for P_{orb}. There is supporting evidence from Casares et al. (2012) for this as well. Differential photometry was also taken using B, V, and R filters. A downward trend is evident in all three of these light curves as well as a greater overall luminosity in B and V than R as expected.

Dillon T. Trelawny
May 2013

THE 2012 OUTBURST OF THE SOFT X-RAY TRANSIENT/BLACK HOLE CANDIDATE SWIFT J1910.2-0546/MAXI J1910-057

by

Dillon T. Trelawny

A thesis
submitted in partial
fulfillment of the requirements for the degree of
Master of Science in Physics
in the College of Science and Mathematics
California State University, Fresno

May 2013

APPROVED

For the Department of Physics:

We, the undersigned, certify that the thesis of the following student meets the required standards of scholarship, format, and style of the university and the student's graduate degree program for the awarding of the master's degree.

Dillon T. Trelawny

Thesis Author

Frederick A. Ringwald (Chair)	Physics
Steven White	Physics
Karl Runde	Physics

For the University Graduate Committee:

Dean, Division of Graduate Studies

AUTHORIZATION FOR REPRODUCTION
OF MASTER'S THESIS

__X__ I grant permission for the reproduction of this thesis in part or in its entirety without further authorization from me, on the condition that the person or agency requesting reproduction absorbs the cost and provides proper acknowledgment of authorship.

_____ Permission to reproduce this thesis in part or in its entirety must be obtained from me.

Signature of thesis author: _____

ACKNOWLEDGMENTS

D.T.T. would like to thank the California State University, Fresno College of Science and Mathematics for a Graduate Research Enhancement Scholarship, which was awarded by Dean Andrew Rogerson and funded by Dr. Tom McClanhan in the Fresno State Foundation grants office and Provost William Covino. Much thanks also goes to the California State University, Fresno Department of Physics for support through a teaching assistantship.

This research used photometry taken at Fresno State's station at Sierra Remote Observatories. Many thanks is extended to Dr. Greg Morgan, Dr. Melvin Helm, Dr. Keith Quattrocchi, and the other SRO observers for creating this fine facility as well as the Department of Physics at Fresno State for supporting it.

This research has made use of the Simbad database and the VizieR Service, which are maintained by the Centre de Données astronomiques de Strasbourg, France as well as NASA's Astrophysics Data System.

TABLE OF CONTENTS

LIST OF TABLES

Page

LIST OF FIGURES

Page

Dedicated to Mom and Dad

INTRODUCTION

X-ray binaries are closely-orbiting binary star systems composed of a compact object and a main sequence companion star. The compact object is either a neutron star or black hole and are thus the more massive cousins of cataclysmic variables, whose compact object is a white dwarf. The companion star is deformed by the stronger gravitational attraction of the compact object. As soon as the outline of this "teardrop-shaped" deformation of the companion's outer layers reaches the critical point for mass to transfer onto the accretion disk, the companion is said to fill its Roche lobe. The easiest point for this to occur is located at the pinnacle of the Roche lobe, also known as the system's inner Lagrangian point, L_1. When the stream of accreted gas strikes the disk it creates a bright spot on the outer edge that is pulled tangentially around the plane of the disk. This bright spot also contributes to the luminosity of the system and can often be seen in light curves of eclipsing systems. X-ray binaries are divided into two main types based on the optical companion properties: high mass X-ray binaries (HMXBs) and low mass X-ray binaries (LMXBs). Figure 1 shows a comparison between HMXBs and LMXBs. There are several excellent reviews of the properties of X-ray binaries, namely Paradijs & McClintock (1995), Seward & Charles (2010), White et al. (1995), Casares (2001), Hellier (2001), and Charles and Coe (2006).

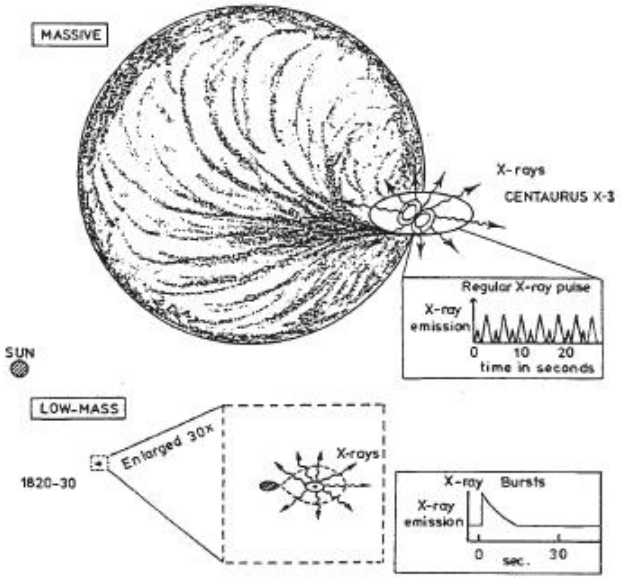

Figure 1. The two types of X-ray binaries: HMXBs and LMXBs. The two insets show the X-ray emission from the respective compact objects. The Sun is included to scale for prospective. From van den Heuvel & Taam (1984).

High Mass X-ray Binaries

HMXBs are characterized by young, luminous OB supergiants with high mass transfer rates ($\dot{m}$) via intense stellar wind (typical $\dot{m} \sim 10^{-6}$ $M_\odot$ yr^{-1}) or Roche lobe overflow (see explanation below). Due to their intense optical emission, the supergiant companion completely overshadows the X-ray emission from the accretion disk and dominates the overall luminosity of the system resulting in a $L_{opt}/L_X > 1$. However, since Swift J1910.2-0546/MAXI J1910.2-0546 (henceforth referred to as Swift J1910) is an LMXB, the focus of this thesis will not be on HMXBs.

Low Mass X-ray Binaries

LMXBs are characterized by a late-type main sequence companion, typically a red dwarf, that is constantly being bombarded by a barage of X-rays from the compact object. The companion absorbs these incident X-rays and reradiates them in the ultraviolet and optical. They typically have $L_{opt}/L_X < 0.1$ with the X-ray flux exhibiting occasional rapid bursts with exponential decays on timescales of ∼30 seconds. These are believed to be a result of thermonuclear explosions on the surface of the neutron star (NS LMXBs). Systems with a black hole as the compact object (BH LMXBs) do not exhibit X-ray bursts since black holes do not have solid surfaces. Therefore, it can be said that these rapid X-ray bursts signify the existence of a neutron star as the compact object. Consequently, this provides an upper limit on the mass of the system of 3 $M_\odot$, which is the maximum allowable mass for a neutron star and the minimum mass required to form a black hole (Casares 2001).

Nomenclature

It would be instructive to explain why these systems are called X-ray binaries and show that their luminosity has sufficient energies to indeed radiate in the X-ray spectrum. The luminosity of the system comes from a combination of the bright spot and the viscosity of the gas as it moves through the accretion disk. A more massive compact object will generally result in a high system luminosity since the gas in the accretion disk will be pulled more quickly onto the compact object. This creates more collisions

between the gas particles, the temperature rises due to this increase in friction and, if occuring across the entire surface area, ultimately results in a higher disk luminosity. This accretion rate $\dot{m}$ of gas onto the compact object is directly proportional to an accretion luminosity:

$$L_{acc} = \frac{GM\dot{m}}{R} \tag{1}$$

where M and R are the mass and radius of the compact object and G is the universal gravitational constant. A lower limit of the X-ray flux can be derived using the lower mass limit for a neutron star of $M \simeq 1.4\mathrm{M}_{\odot}$, $R \simeq 10$ km, and a typical $\dot{m} \simeq 10^{16}$ g s^{-1}, resulting in an accretion luminosity $L_{acc} \sim 10^{36}$ erg s^{-1}. If the compact object is assumed to absorb and reradiate precisely all of the incident radiation, known as a blackbody, we can estimate the temperature of the compact object and thus determine the energy of the radiation emitted. The accretion luminosity may also be written in terms of the neutron star's temperature as:

$$L_{acc} = 4\pi R^2 \sigma T^4 \tag{2}$$

where σ is the Stefan-Boltzmann constant. Using a typical neutron star radius of $R \simeq 10$ km results in a temperature of $T \simeq 10^7$ K. A typical photon at this temperature has an energy $kT \simeq 1$ keV, where k is the Boltzmann constant. Thus, we have a put a lower limit on the energy of emitted radiation of $\simeq$1 keV from a typical binary star system containing a neutron star, which is consistent with radiation in the X-ray spectrum.

Soft X-ray Transients

There is a special type of LMXBs that exhibit immense, rapid X-ray outbursts lasting several days and gradually decay back into quiesence over several months. These star systems are called soft X-ray transients (SXTs), sometimes referred to as X-ray novae, and have recurrence times believed to last from several decades to several centuries. Currently, ∼25% of all SXTs are confirmed neutron star systems with the remainder being black hole candidates (Charles & Coe 2006). The reason for this is because in neutron star systems the outer regions of the disk are irradiated more than in systems with black holes, due to the fact that there is no definite surface to a black hole. When accreted gas reaches the black hole it simply disappears without the creation of radiation. Thus, the outer disk regions of black hole systems exist in cooler and more un-ionized states, which leads to the buildup of more gas over longer timescales and eventually the outburst. This is why a majority of SXTs contain black holes rather than neutron stars.

The leading theory of the origin of outbursts in SXTs is attributed to the disk (thermal) instability, which has been modeled and theorized for decades. Photons are tiny quanta of electromagnetic radiation that interact strongly with charged particles and weakly with neutral atoms. This phenomenon is illustrated in an accretion disk. Cool, un-ionized hydrogen gas has a low opacity, or in other words only weakly inhibits the flow of radiation. Contrarily, hot, ionized hydrogen has a high opacity and does not allow photons to flow easily. If the temperature of the gas is increased to ∼7,000 K, the hydrogen atoms will begin to ionize, resulting in a higher opacity.

However, more energy is spent in ionizing rather than heating the gas. So in partially-ionized gas opacity is very sensitive to temperature (see Section 5.3 of Hellier 2001).

Now consider an SXT accretion disk. A small rise in the local temperature of some region in the disk will result in a higher opacity and viscosity and slowing down the particle velocities. The gas particles in this region will fall inwards to a smaller radius from a need to conserve angular momenum, thus opening up a less dense region of lower opacity and viscosity. With a small temperature increase, the opacity increases dramatically. Heat is trapped in the opaque region due to the increased viscous interations and further increases the temperature. The overall picture is that the energy trapped in this newly-dense region far outweighs the heat that is trapped in the same region. There is a snowball effect that continues to permeate the disk until the system reaches a new quasi-equilibrium. If the amount of gas entering the disk via Roche lobe overflow from the secondary is insufficient to maintain the system in this hot, viscous state, then the system goes into outburst and returns to its original state. As the regions of hot, viscous gas move inwards, a cooling wave follows. In SXTs, irradiation from the compact object causes this cooling wave to more inwards on a much longer timescale, effectively pushing against its inward motion. This is believed to be the reason why the quiescent intervals among SXTs are so prolonged (Charles & Coe, 2006).

The companion dominates the optical emission of the system, with typical quiescent magnitudes of $V \sim$ 16-23. The light curves typically show

erratic, aperiodic flickering behavior with amplitudes of ∼0.2 magnitudes. Light curves are plots of intensity (W/m^2), usually measured in astronomy as apparent magnitude, as a function of time. The flickering is thought to arise from the turbulent nature of the accretion disk as clumps of gas randomly strike the surface of the neutron star. The light curves of SXTs have three primary characteristics: a sharp rise, an exponential decay, and the presence of secondary maxima typically occurring ∼50 and ∼170 days after initial outburst. Figure 2 is the light curve from the first SXT system discovered, designated A0620-00 in 1975, showing its outburst as well as the secondary maxima as the system decays back into quiescence.

Origin of the Secondary Maxima

A plethora of theories have been proposed attempting to explain the origin of these "rebrightenings." The most popular mechanism to explain this phenomenon is the disk instability model by Cannizzo, Wheeler, & Ghosh (1985). Upon initial outburst, the intensity of the X-ray emission increases by $\sim 10^6$, whereas the optical intensity increases by $\sim 10^3$. In addition, there is a stronger emission of *hard* X-rays (>5 keV) than *soft* X-rays (∼0.1 keV−5 keV). The hard X-rays decay much faster than their soft counterparts comprising only 1% of the total flux remaining after ∼60 days (Mineshige 1994). During an outburst, a Compton cloud is formed in the inner region of the accretion disk near the compact object. This Compton cloud is essentially a region of very hot, dense, ionized gas that scatters any photons that pass through. This cloud envelopes the inner accretion disk as well as the spherical

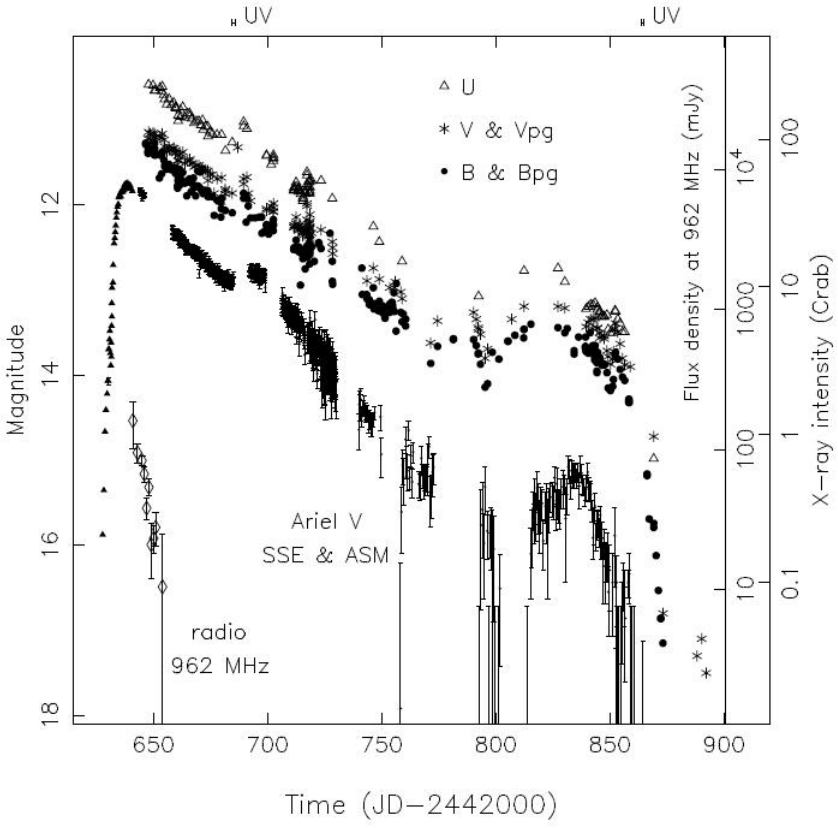

Figure 2. Multiwavelength light curve of the prototype SXT A0620-00 during its 1975 outburst showing the amplitudes of the secondary maxima at ∼50 days and ∼170 days. From Kuulkers (1998).

inner coronal region above and below the compact object. During the first several weeks of the outburst, hard X-rays emitted from the compact object due to the infall of gas are blocked from escaping to the outer regions of the disk resulting in a majority of the observed X-ray flux being in the soft regime. Once the hard X-ray flux sufficiently diminishes, the Compton cloud evaporates, enabling the hard X-rays to irradiate the outer regions of the disk and thereby causing secondary heating (Mineshige et al., 1994).

There are two primary results of this second heating phase. First, the companion star is irradiated, causing its surface to heat up, which results in an increased $\dot{m}$. Second, since LMXBs tend to have flared accretion disks, the upper and lower rim of the flared outer disk is X-ray irradiated. The middle regions of the outer disk are believed to be blocked from irradiation by the disk itself. The X-ray irradiation of gas in the outer regions of the disk increases the temperature of the gas. This increase in temperature comes with an increase in the viscosity of the gas moving around the disk. A higher viscosity causes the gas to lose angular momentum and fall in towards the compact object. If this occurs across the entire disk, then there arises a collective heating wave that moves inward at essentially the same rate and will result in a second outburst observable from the optical to X-ray wavelengths. The entire process is then repeated and is the reason for the rebrightening seen at $\sim$170 days in the light curves of SXTs (Seward & Charles 2010).

A Brief History of Observations

As discussed earlier, the nature of soft X-ray transients is that their outbursts may be separated by decades, which makes observing the same system through two consecutive outbursts a fairly long and drawn out affair. This made for exciting times on the night of 2012 May 30-31 when X-rays first spewed forth and sent astronomers scrambling for observations. Notices of these observations were posted online using The Astronomer's Telegram. The following sections descibe some of the major observations of Swift J1910 so far.

ATel #4145

Kennea et al. (2012) reported observations of Swift J1910 on 2012 June 4. No QPOs were detected and they proposed that Swift J1910 was still in the "thermal" state, which was consistent with no QPO activity (Remilliard & McClintock 2006).

ATel #4146

On 2012 June 1, Cenko et al. (2012), on behalf of the Palomar Transient Factory, reported observations of the optical counterpart of Swift J1910 using an R band filter at a magnitude of $R = 15.9$.

ATel #4195

Britt et al. (2012) observed Swift J1910 for three nights over 2012 June 1-4 using the 0.9m SMARTS Consortium telescope at the Cerro Tololo Inter-American Observatory in Chile. They reported optical variability in the counterpart of $r' = 15.50 \pm 0.01$ on June 1, $r' = 15.42 \pm 0.01$ on June 3, and $r' = 15.40 \pm 0.01$ on June 4. These magnitude values are the averages of the data taken on those nights. They also reported dominant flickering activity of up to 0.1 magnitudes that is evident in all their observations on timescales of up to an hour. They did not report any significant periodicities in their data.

ATel #4198

Kimura et al. (2012) reported that Swift J1910 was observed to be in a

bright soft state and exhibited a soft-to-intermediate X-ray state transition. On 2012 June 10-12, they observed the 2-4 keV X-ray flux reached a peak of 2 Crab, or ∼4.8 x 10^{-8} ergs cm^{-2} s^{-1}. A Crab (or mCrab) is a unit of astrophotometric measurement used in X-ray astronomy based on the X-ray flux of the Crab nebula at corresponding energies (the Crab nebula's intensity varies at different X-ray energies). They report the 2-4 keV flux decreased from 2012 June 16-21, the 4-10 keV flux remained approximately constant, and the 10-20 keV flux tended to increase. These trends indicate a soft-to-intermediate transition has taken place. In other words, the flux of lower energetic X-rays is getting smaller while the flux from the more energetic X-rays is getting more intense.

ATel #4246

Lloyd et al. (2012) report time-series photometry taken with 0.35m to 0.5m class telescopes in Australia, Chile, and the United Kingdom. They obtained V band observations on 2012 June 27, 28, and 29, and July 1, 6, and 7. They reported the mean V magnitude faded from $V = 15.83$ to $V = 15.98$ with various modulations up to 0.3 magnitudes. They performed a Lomb-Scargle periodogram analysis to search for periodicities and found a clear set of peaks centered near a frequency of 10.75 cycles/day with a weaker set near 4.00 cycles/day (these values match our data reasonably well; see Data Analysis section). They did not report any flickering activity.

ATel #4273

Nakahira et al. (2012) reported follow-up observations of Swift J1910 in which they proposed that Swift J1910 was going through the soft-to-hard state transition. They reported that the 2-4 keV flux decreased slightly from 310 ± 16 mCrab to 270 ± 13 mCrab, while the 4-10 keV flux increased from 33 ± 8 mCrab to 77 ± 8 mCrab and finally to 112 ± 12 mCrab. They suggested that this behavior between the two energy regimes signified that Swift J1910 was going through the soft-to-hard state transition, which is evident in soft X-ray transients.

ATel #4295

King et al. (2012) reported the first radio detections of Swift J1910 from 2012 August 3 with the Jansky Very Large Array. The source was detected at 2.5 milliJanskys (mJy) at 6 gigaHertz (GHz), where 1 Jansky = 10^{-26} W m^{-2} Hz^{-1}. In essence, this corresponds to a rather small detection level over a very narrow frequency bandwidth. These were the first documented radio observations of Swift J1910.

ATel #4328

Bodaghee et al. (2012) reported observations of Swift J1910 emitting in the hard X-rays using INTEGRAL's hard X-ray imager (ISGRI). From data taken on the night of 2012 August 20-21, the system was detected in the 18-40 keV range at a high significance level of 13.7σ and in the 40-100 keV range at a significance level of 9.4σ. ISGRI also detected Swift J1910 up to energies of ∼200 keV. These detections confirmed that Swift J1910 was indeed

in the hard state.

ATel #4347

Casares et al. (2012) reported on R band photometry of Swift J1910 of over 3.1 hours on the night of 2012 July 21 using the 2.5m Nordic Optical Telescope. They measured a mean magnitude of $R = 16.20$. This is in slight disagreement with our own R band observations shown in Figure 31 that give a mean magnitude of $R \sim 15.76$ during this same night, which, luckily enough, was our final night of R band observations. For a further discussion of our calculated B, V, and R magnitudes see the B, V, & R Photometry section. In addition, they proposed an orbital period of >6.2 hours due to spectroscopic radial velocity observations of Hα emission from the optical counterpart. This appears to be the lowest frequency periodicity seen in Figures 11, 16, 20, and 25, which we propose may resemble either the precessional period or the orbital period of the system.

OBSERVATIONS

Time-resolved differential CCD photometry was carried out beginning on the night of 2012 June 21-22 UT and continued until 2012 September 19-20 UT. In this time, we collected 43 nights of data, 41 of which were included in our analysis. The night of 2012 July 2-3 was unusable because of the proximity to the Full Moon and the night of 2012 August 26-27 unusable due to complications in the data reduction. Table 2 is a journal of our observations.

We used the 0.41m (16 in) f/8 telescope by DFM Engineering at Fresno State's station at Sierra Remote Observatories and a Santa Barbara Instruments Group STL-11000M CCD camera. Frames were exposed for 120 seconds with a dead time to read out the CCD between exposures of 7 seconds, making for a total time resolution of 254 seconds. Due to the target being a soft X-ray transient, its brightness was gradually diminishing and, in the later months, required a longer exposure time. In order to ensure we continued to collect enough light, we increased the exposure time from 120 seconds to 180 seconds beginning on 2012 August 31-September 1 and ulitmately to 240 seconds on 2012 September 13-14, which continued through the rest of our observations. The dead time for each exposure remained at 7 seconds, making for a new time resolution of 494 seconds.

All exposures were taken through a Clear luminance filter by Astrodon. The Clear filter allows for the maximum amount of light to enter the CCD camera, which is optimal since our target is very faint at approximately 16^{th}-17^{th} magnitude. Weather was clear and apparently

photometric on most nights. However, there were a few nights that appeared to be marginally obscured by clouds or haze.

All data were processed with AIP4WIN 2.1.8 software (Berry & Burnell, 2005). All exposures were dark-subtracted, but not divided by a flat field. The CCD temperature was set to -5°C for all exposures. Fifteen dark frames were collected every night. These dark frames were median-combined to form a master dark frame, which was then subtracted from each of the target frames.

To measure the photometry we used comparison and check stars that are preferred by the British Astronomical Association Variable Star Section (BAAVSS), who first observed the target on 2012 June 14 (Pickard 2012). Figure 3 is the finding chart provided by the BAAVSS and the comparison and check stars that we used are labeled as $C4$ and $C5$, respectively. Note that the designations by the BAAVSS of the comparison and check stars as $C4$ and $C5$, respectively, are different from the designations that we use for the comparison and check stars as $C1$ and $C2$, respectively, in our plots. The BAAVSS used the Carlsberg Meridian Catalogue 141 (CMC 14) names, so in order to determine the magnitudes in the other filters the Two Micron All Sky Survey (2MASS) was consulted. Table 1 lists the CMC 14 and 2MASS designations of V, $C4$, and $C5$ as well as their magnitudes in each filter.

Our telescope and camera have an image scale of 0.51 arcseconds/pixel. All of our observations were done using 3x3 binning, making for an image scale of 1.53 arcseconds/pixel. All photometry used an aperture of 6 pixels, or 3.06 arcseconds, in diameter, and used inner and outer

annuli of 9 and 11 pixels, or 4.59 and 10.61 arcseconds respectively, in diameter for sky subtraction. Figure 4 shows a typical nightly light curve of our differential photometry of Swift J1910 as well as the comparison (C1) and check (C2) stars for the night of 2012 June 21-22.

CMC 14	2MASS	B	V	R	r'
Swift J1910	-	16.70	16.00	15.64	-
J191028.2-054652	19102823-0546524	14.80	13.762	13.20	13.535
J191011.7-055026	19101170-0550266	15.00	14.255	14.10	14.050

Table 1. Designations as well as B, V, R, and r' magnitudes of Swift J1910, the comparison (C4) and the check stars (C5) used in our photometry. Swift J1910 is not included in the 2MASS database.

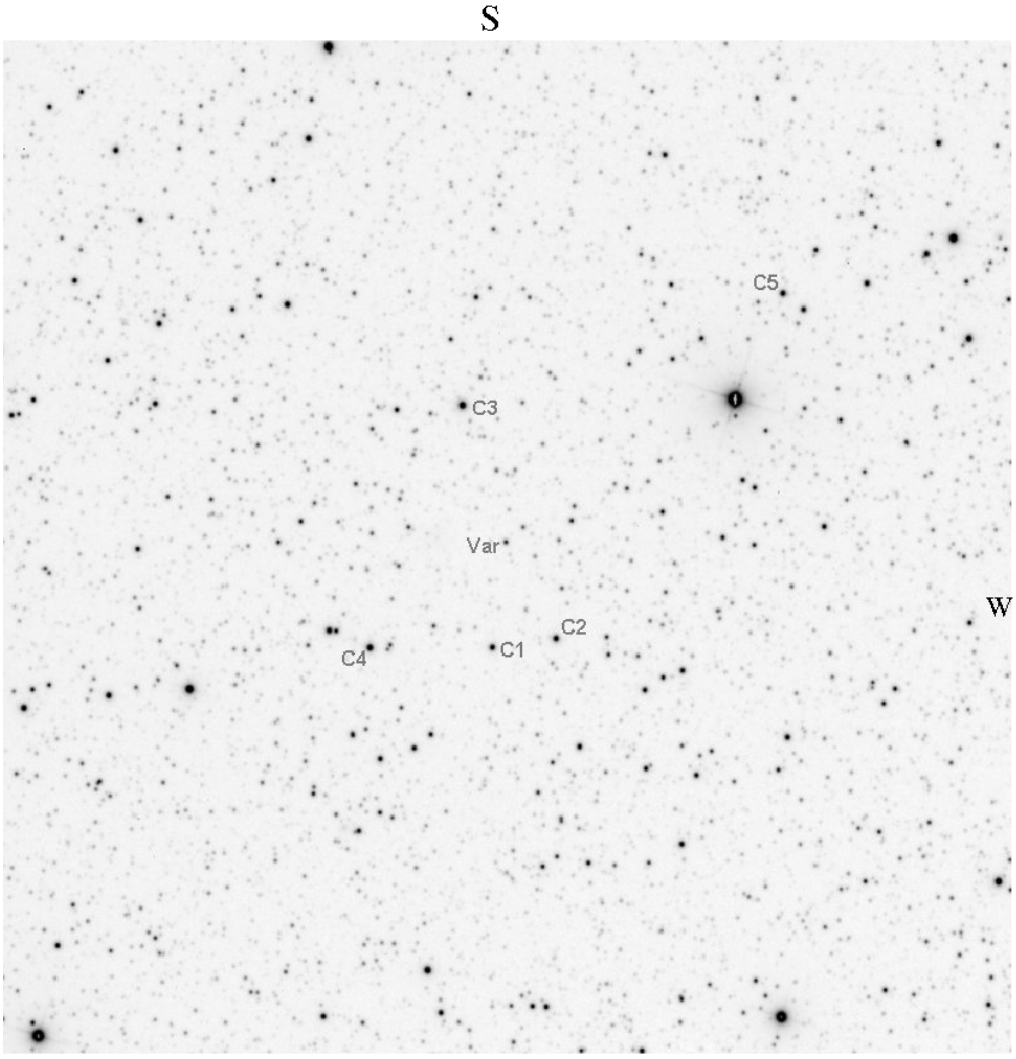

Figure 3. Finding chart for Swift J1910 showing the comparison (C4) and check (C5) stars, provided by the British Astronomical Association Variable Star Section (Pickard 2012). The field of view is 15 arcminutes square.

Night	2012 Date	UT Start	Duration (h)	Exposure #	Seeing ($''$)
1	June 21-22	5:59	5.64	160	1.35
2	June 22-23	5:19	6.35	180	1.41
3	June 23-24	5:30	1.09	31	1.25
4	June 24-25	6:35	4.94	140	1.18
5	June 25-26	4:59/9:34	6.21	120/56	1.58/1.13
6	June 26-27	5:01/7:14/9:13	6.10	56/50/67	1.79/1.11/0.76
7	June 27-28	4:55/7:09/9:55	6.23	59/72/47	1.25/0.99/0.97
8	June 28-29	5:08/7:10/9:15	5.89	51/51/65	0.96/0.96/-
9	June 29-30	5:05/7:12/9:16	5.50	49/42/65	2.31/1.19/1.09
10	June 30-July 1	5:02/7:11/9:10	6.28	56/52/70	1.45/1.04/0.99
11	July 1-2	5:25/7:08/9:09	5.89	44/52/71	0.95/1.20/1.30
12	July 6-7	4:57/7:10/9:09	6.35	58/52/70	1.15/1.07/0.91
13	July 7-8	6:43/8:45	4.80	51/85	1.34/1.14
14	July 8-9	5:20/8:41	4.41	90/75	1.10/0.95
15	July 9-10	4:38/7:11/9:11	6.70	68/52/70	1.30/1.20/1.50
16	July 10-11	4.34/7:08/9:11	6.70	68/54/68	1.60/1.10/1.25
17	July 13-14	5:37/8:32	5.86	58/68	1.09/1.15
18	July 14-15	4:12/8:43	6.99	122/76	1.40/1.21
19	July 15-16	4:24/7:30	6.91	82/114	1.87/1.24
20	July 16-17	5:48/8:32	5.36	73/79	-
21	July 17-18	5:33/7:50	4.97	60/81	1.19/1.20
22	July 19-20	4:53/7:25	5.36	67/85	-
23	July 20-21	4:41/7:19	5.68	65/96	1.25/1.49
24	July 21-22	4:14/7:58	6.46	100/83	1.03/1.04
25	August 23-24	4:45	4.52	128	-
26	August 24-25	3:25	4.97	141	-
27	August 25-26	3:39	4.97	141	-
28	August 29-30	3:42	4.13	117	1.01
29	August 31-Sept. 1	3:44	3.84	74	0.87
30	Sept. 1-2	4:17	4.00	77	-
31	Sept. 2-3	4:00	4.21	81	1.34
32	Sept. 3-4	4:18	3.74	72	1.16
33	Sept. 4-5	3:34	4.26	82	1.18
34	Sept. 7-8	3:10	4.60	67	-
35	Sept. 13-14	3:56	3.22	47	1.24
36	Sept. 14-15	3:18	4.05	59	1.00
37	Sept. 15-16	4:20	2.95	43	1.20
38	Sept. 16-17	8:45	3.09	45	1.25
39	Sept. 18-19	3:31	3.43	50	1.39
40	Sept. 19-20	3:24	3.84	56	1.20
41	Sept. 20-21	2:57	3.91	57	1.30

Table 2. Swift J1910 Journal of Observations.

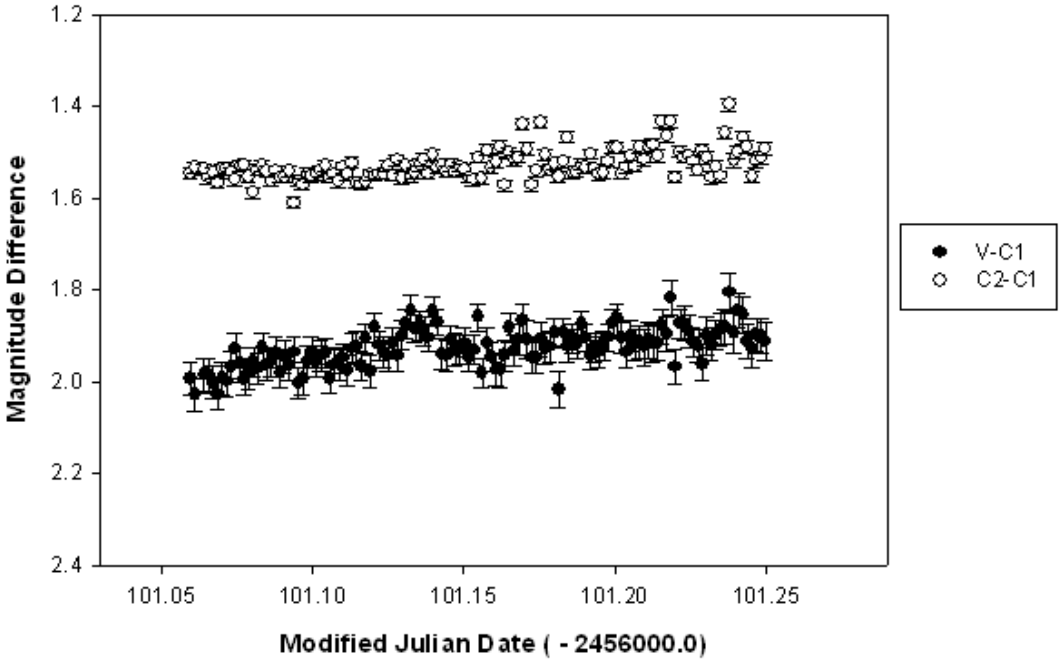

Figure 4. Differential light curve of Swift J1910 for 2012 June 21-22.

DATA ANALYSIS

Figure 5 shows the differential light curve of all 41 nights used in our analysis. Swift J1910 was discovered to have gone into outburst on the night of 2012 May 30-31 simultaneously by the hard X-ray transient monitor aboard NASA's Swift Burst Alert Telescope on NASA's Swift Gamma Ray Observatory and Monitor of All-sky X-ray Image (MAXI) aboard the International Space Station. Since our observations began on 2012 June 21-22, we note a gradual downward trend in the optical $V - C1$ light curve as well as a definite rise, or rebrightening, $\sim$190 days after initial outburst. This secondary maxima, at $\sim$50 and $\sim$170 days, are characteristic features of soft X-ray transients. We suspect that the first rebrightening at $\sim$50 days occurred during the hiatus in our observations and that the bump we see in our light curve beginning around 2456170 Julian days (JD), or August 30, is actually the second rebrightening.

We excluded several nights because of occasional fluctuations such as passing satellites or cosmic rays incident on the CCD detector that were outliers in the light curve and would have otherwise biased our data. No obvious periodicities could be determined from the periodogram analysis of all 41 nights, which was dominated by strong aliasing due to so many gaps in our observations (see Box 9.1 of Hellier, 2001). To try and overcome this, we divided the data set into two observing sessions in hopes of determining more accurate periodicities. Figure 6 shows how the two observing seasons compare with one another. We list the $V - C1$ light curves for both observing seasons

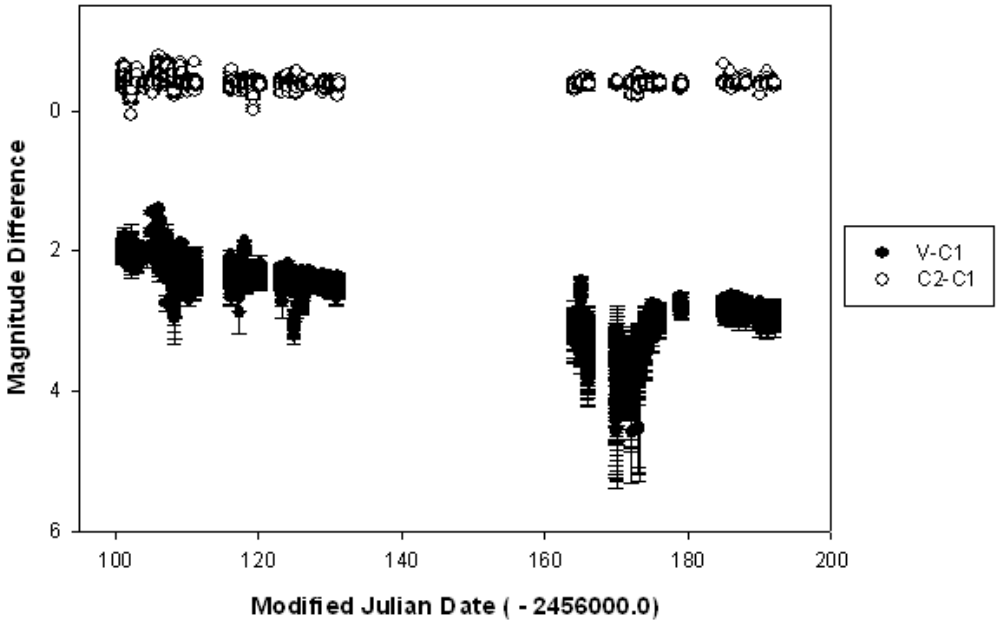

Figure 5. Differential light curve of Swift J1910 for all 41 nights.

with their respective Lomb-Scargle (L-S) periodograms (Lomb 1976; Scargle 1982; Press et al., 1992) that we calculated with the PERANSO (PEriod ANalysis SOftware) software package (Vanmunster, 2009), and spectral window functions (SWFs). Light curves are plots of intensity, measured as apparent magnitude and typically having units of W/m^2 as a function of time. The $V - C1$ curve shows how much the intensity of the variable (Swift J1910 in this case) changes when compared to a companion star. The $C2 - C1$ curve should be as flat as possible in order to prove that the intensity of the companion star does not change as well. Thus, by direct comparison of both curves, any variability of Swift J1910 can be seen. A L-S periodogram is used to search for periodicities in the light curves. The spectral window function

shows how the sampling rate affects our periodogram due to convolution with the diurnal cycle. For instance, if observations were made every night for 6 hours for one week, the SWF would show a strongest peak at 1 cycle/day and less prominent peaks at 2 cycles/day, 3 cycles/day, etc. For a more detailed discussion of the convolution theorem and the diurnal cycle see Press et al. (1992). There are no definite periodicities that can be seen in either periodogram. The periodogram for Weeks 1-5 has strong peaks at 0.025, 1.019, and 2.021 cycles/day and the periodogram for Weeks 10-15 has strong peaks at 0.027, 0.970, and 1.976 cycles/day. Since these frequencies are all separated by $\sim$1 cycle/day, they should not be trusted as true variability due to the strong probability of being biased from observing on consecutive nights.

Additionally, all peaks in the SWFs align with all peaks in the periodograms, which tells us that those periodicities arise from our sampling rate. If there were peaks in the periodogram that did not have a corresponding peak in the SWF at the same frequency, then this would indicate variability due to optical modulation in the accretion disk. Each strong peak in the periodogram is accompanied by smaller peaks on each side. These smaller peaks are aliases since they repeat with every strong peak in the periodogram and thus cannot be construed as true variability.

Since no periodic variability could be determined from the light curves of the two observing seasons individually, we further divided the data into five sections. These sections were chosen based on the number of consecutive nights of observations, since it is preferred to have as many consecutive nights as possible for the periodogram analysis.

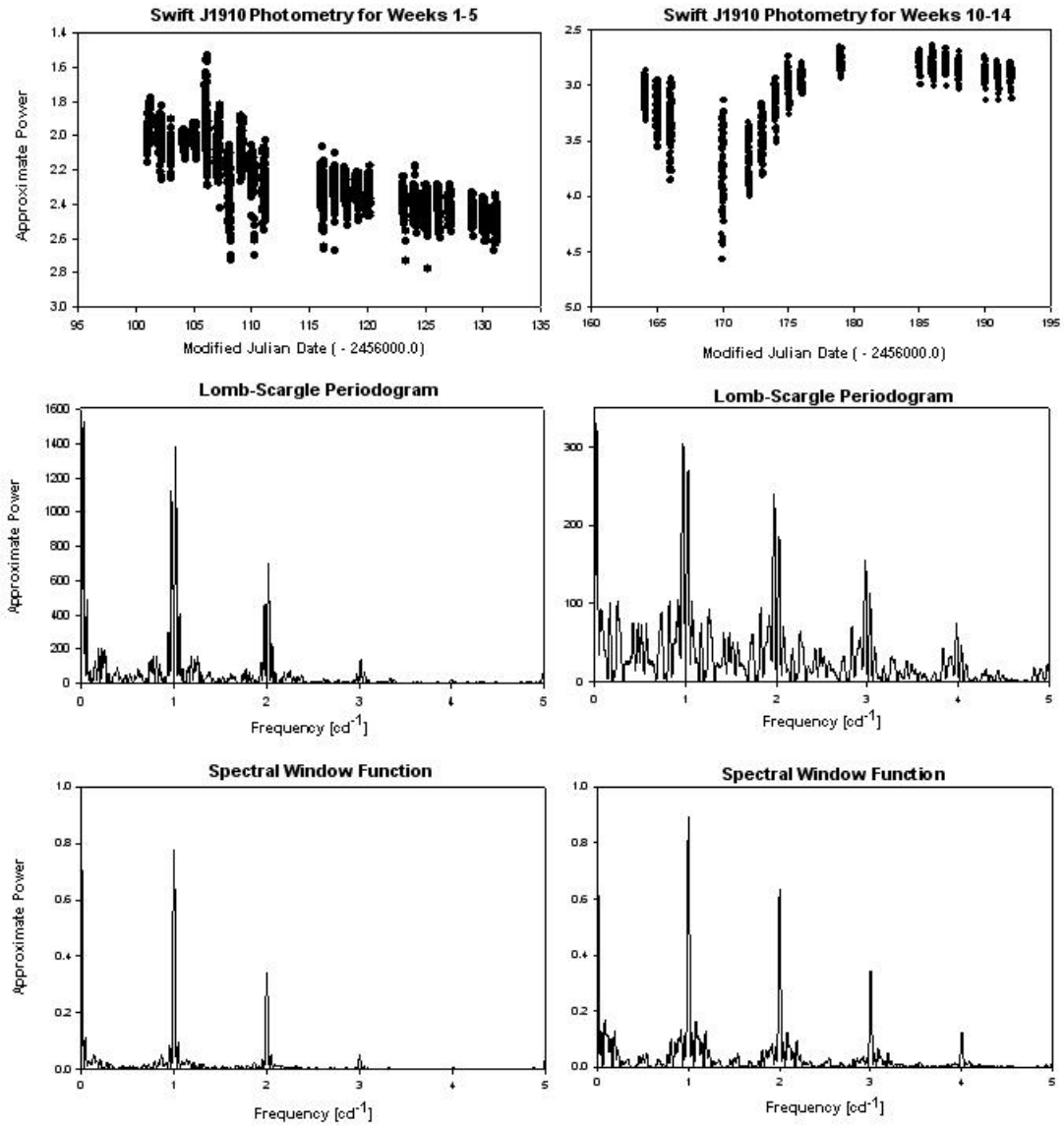

Figure 6. The two primary observing seasons and their respective light curves (top), Lomb-Scargle periodograms (middle) and spectral window functions (bottom). LEFT: June 21-22 until July 21-22; RIGHT: August 23-24 until September 20-21. There are no true periodicities in either observing season, only those due to aliasing.

1. Nights 1-11

The first section is comprised of the first eleven nights of observations, 2012 June 21 to July 2. Figure 7 is the L-S periodogram and Figure 8 is the corresponding spectral window function. We note four distinct periodicities with frequencies of $F_1 = 0.064 \pm 0.012$ (15.649 d), $F_2 = 0.942 \pm 0.001$ (25.483 d), $F_3 = 1.072 \pm 0.0017$ (22.39 h), and $F_4 = 2.059 \pm 0.002$ (11.656 h) cycles/day. When compared to Figure 8, we can see that F_1, F_3, and F_4 are factors of the sampling rate and so may be disregarded. The tiny periodicity at F_2 is believed to be a spurious peak, since it does not repeat in later periodograms. We attribute the system still being highly irradiated from its outburst approximately three weeks before to be the reason why there were no distinct periodicities detected in the first eleven nights of observations. In addition, note the lack of low-amplitude flickering in the light curve, which we also attribute to the system still being highly irradiated. If Swift J1910 is optically bright, then detection of high-frequency fluctuations in the light curve would prove difficult. This is due to the brightness of the rapid fluctuations being masked by the greater brightness of the system as a whole. The peak at $F = 672$ cycles/day is the Nyquist frequency, or the highest frequency possible to obtain an accurate fit to our data (Press et al., 2002).

Since Fourier analysis can omit signals, such as high frequency optical quasi-periodicities, that are aperiodic in amplitude and frequency (see Papadaki et al., 2006) we applied the following procedure to attempt to enhance any such signal. The L-S periodogram was averaged over the eleven

nights, then plotted on a log-log scale. Figure 10 shows the resulting average power spectrum. It shows that a majority of the maximum power is at frequencies <1 cycle/day as well as an absence of high-frequency oscillations. The spike at the far right is a result of the Nyquist frequency. Figures 9 and 10 reinforce our conclusion that there were no distinct periodicities in the first eleven nights of observations, due to the immense irradiation shortly after outburst.

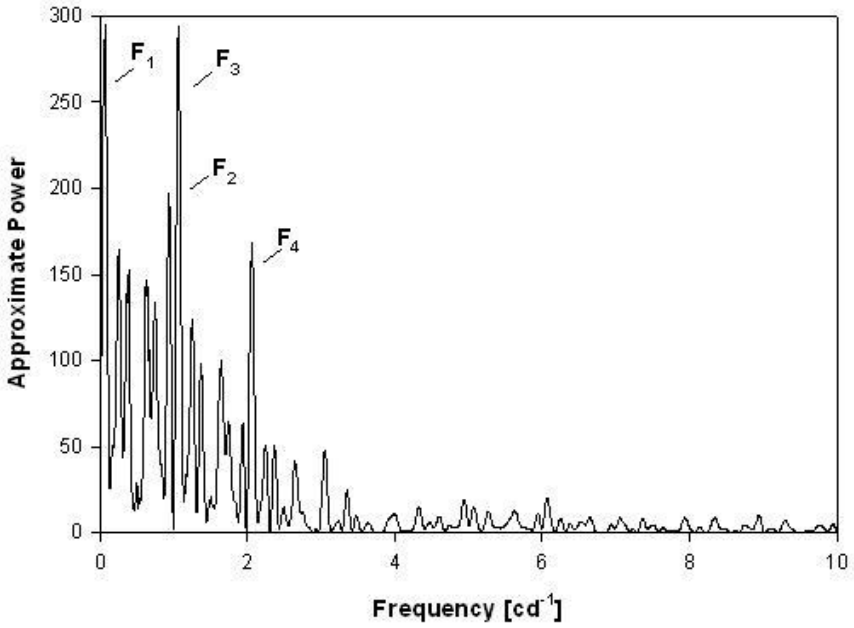

Figure 7. The L-S periodogram for the nights of 2012 June 21 to 2012 July 2.

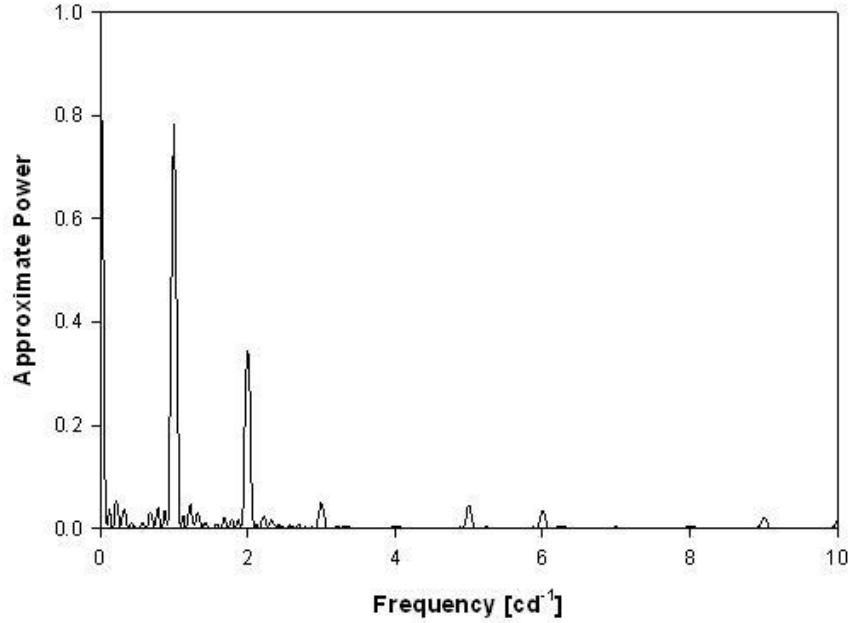

Figure 8. The spectral window function for Figure 7.

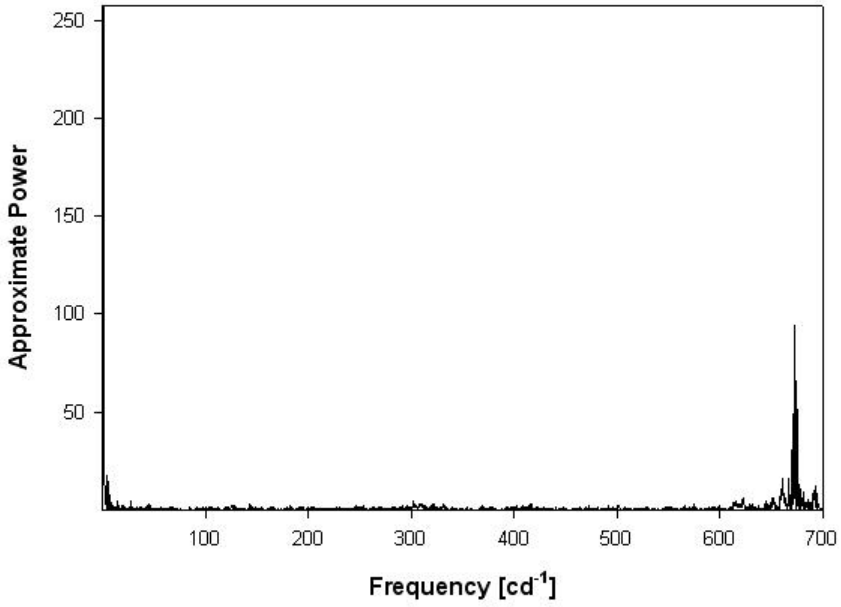

Figure 9. The full L-S periodogram for nights 1-11 of observations. Note the absence of any obvious periodicity. The peak at ∼670 cycles/day is from the Nyquist frequency.

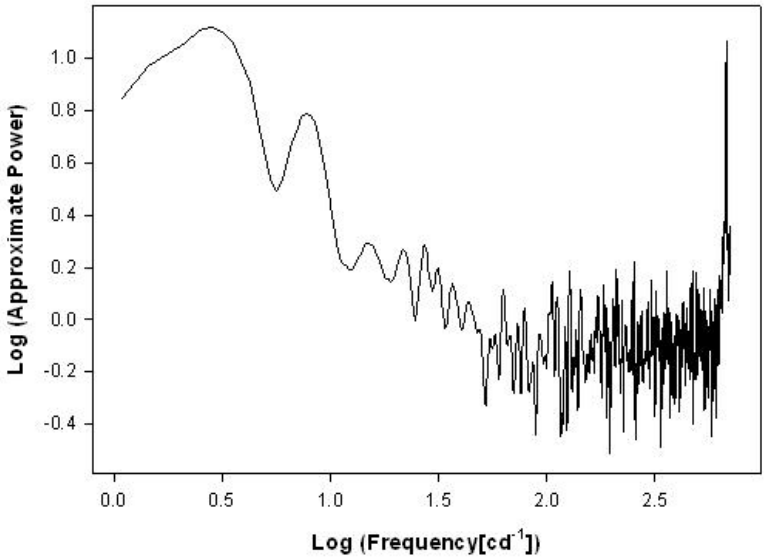

Figure 10. The average power spectrum for nights 1-11 of observations.

2. Nights 12-16

The next group of consecutive observations was nights 12-16, or 2012 July 6-11. Figure 11 is the L-S periodogram and Figure 12 is the corresponding SWF. The periodogram shows prominent frequencies of $F_1 = 2.9565 \pm 0.0999$ cycles/day, corresponding to a period of 8.117 ± 0.011 h and $F_2 = 10.7472 \pm 0.0038$ cycles/day, corresponding to a period of 2.2331 h. Notice that the peaks in the SWF do not correspond to the prominent peaks in Figure 11, which means that frequencies F_1 and F_2 are real variabilities in Swift J1910. Figure 13 shows the light curve folded over the most prominent frequency of 2.9565 cycle/day (8.117 h).

Figure 14 shows higher levels of aperiodic flickering than in the L-S periodogram for nights 1-11 shown in Figure 9. We believe this to be from the disk becoming less irradiated over time and allowing the optical light to be more easily observed. The Nyquist frequency at $F = 670$ cycles/day is also included for completeness. There is a quasi-periodicity candidate at a frequency of 343.534 cycles/day, or $\sim$4.19 min, which is roughly 40% stronger than the surrounding mean noise level. Figure 15 shows the average power spectrum calculated as described earlier. There is a large amount of low-frequency variability present in the data for these nights. A distinct spike at $\log(F \text{ cycles/day}) = 2.536$ matches the signal found in the L-S periodogram in Figure 14. Since this signal remains after calculation of the average power spectrum, I conclude this 4.19 min quasi-periodicity to be real.

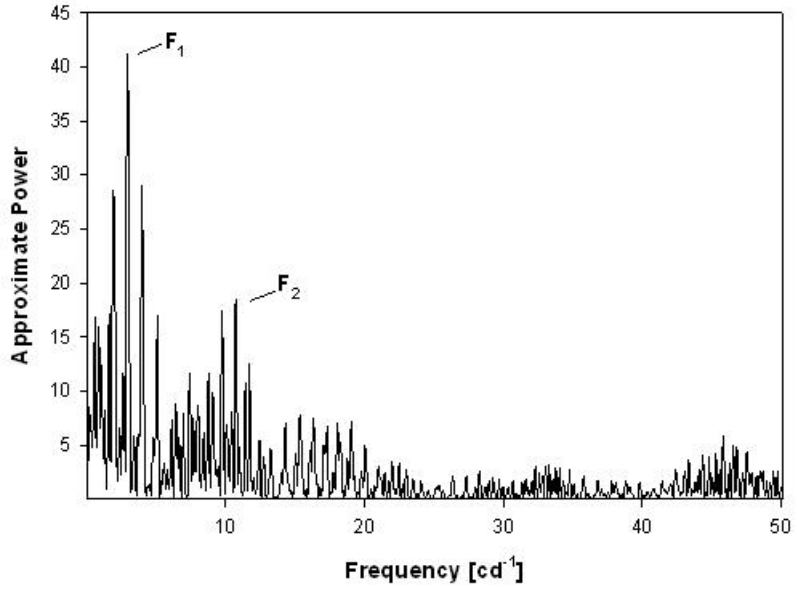

Figure 11. The L-S periodogram for nights 12-16 of observations.

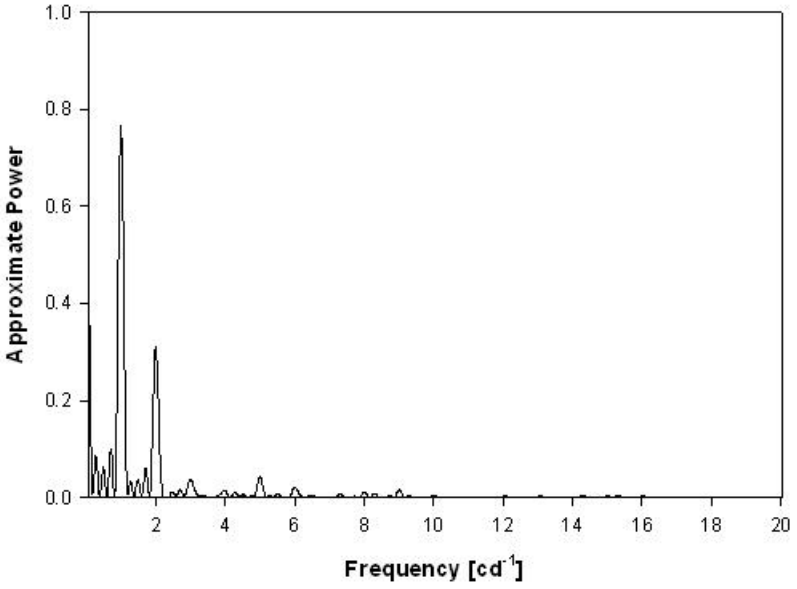

Figure 12. The spectral window function for nights 12-16 of observations.

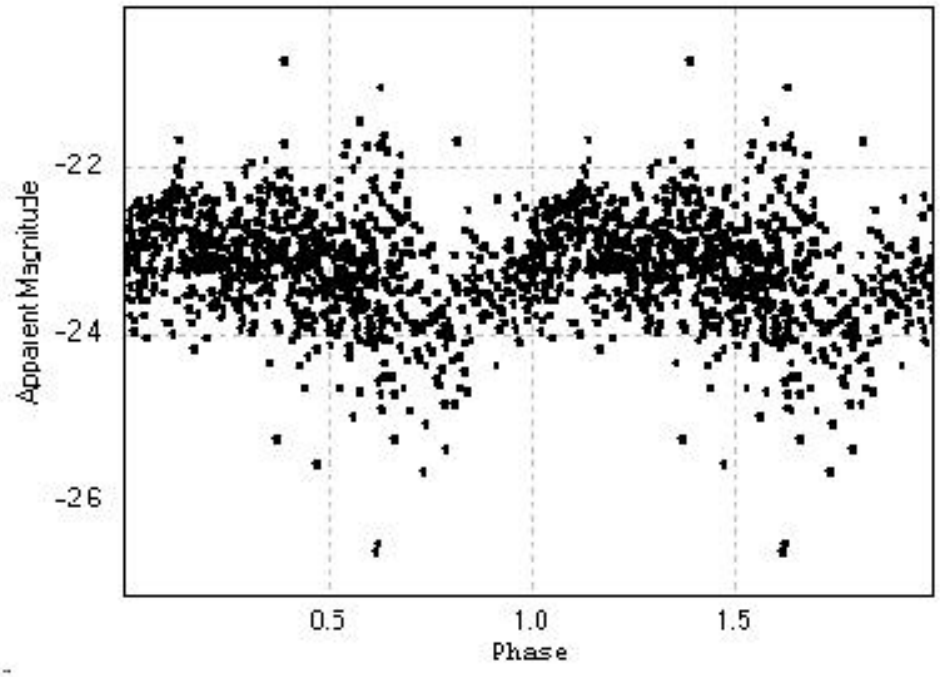

Figure 13. Phase-folded light curve over the proposed orbital period of 8.117 h.

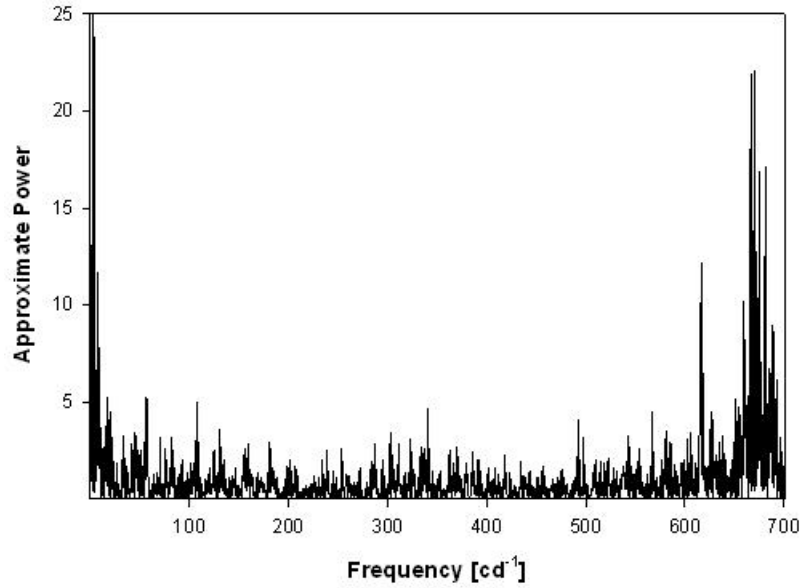

Figure 14. The full L-S periodogram for nights 12-16 out to the Nyquist frequency.

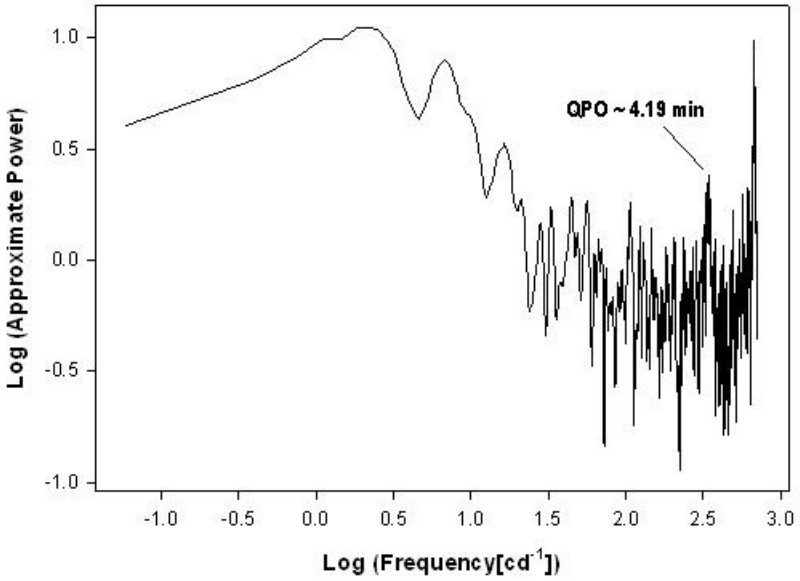

Figure 15. The average power spectrum of the light curve from nights 12-16. A 4.19 min quasi-periodicity candidate is shown at $\log(F) = 2.536$.

3. Nights 17-21

The third section comprises nights 17-21, or 2012 July 13-18. Figure 16 shows prominent frequencies at $F_1 = 3.039 \pm 0.060$, $F_2 = 10.749 \pm 0.006$, and $F_3 = 11.7665 \pm 0.0074$ cycles/day, corresponding to periods of $P_1 = 7.897 \pm 0.007$ h, $P_2 = 2.233$ h, and $P_3 = 2.039$ h, respectively. The strongest frequencies in both Figure 11 (2.9565 cycles/day) and Figure 16 (3.03903 cycles/day) are within the calculated error. This provides strong evidence for this to be a true periodicity in Swift J1910, namely the precessional period or the orbital period. Figure 18 shows the light curve folded over F_1 resulting in strong sinusoidal behavior. There is also the presence of $\sim$10.75 cycles/day frequencies in both periodograms. Lloyd et al. (2012) reported the presence of this same periodicity in their observations of Swift J1910 on 2012 June 27, 28, and 29, and July 1, 6, and 7. However, they report that this is the dominant frequency with weaker peaks near 4 cycles/day, which is contrary to our data. Despite this, we tend to lean towards our data being more accurate since we have a more complete and coherent data set. As further evidence, Casares et al. (2012) put a mimimum constraint on the orbital period of >6.2 h as a result of their spectroscopic radial velocity study of Hα emission. From the evidence outlined above, we argue that the 7.807 ± 0.006 h signal is most likely the orbital period of Swift J1910.

Figure 19 shows the L-S periodogram including the Nyquist frequency at $F = 671$ cycles/day. There are no distinct high-frequency oscillations, since all the peaks are within the mean noise level.

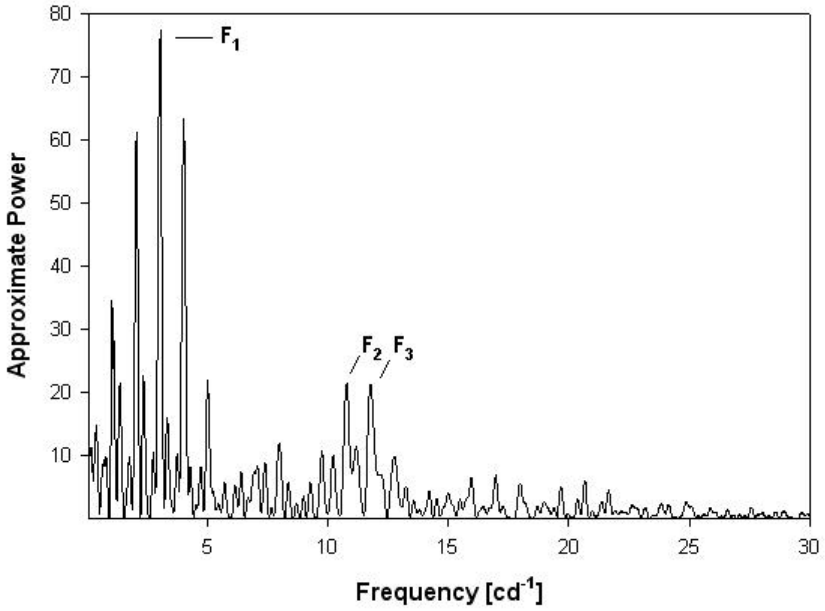

Figure 16. The L-S periodogram for nights 17-21 of observations.

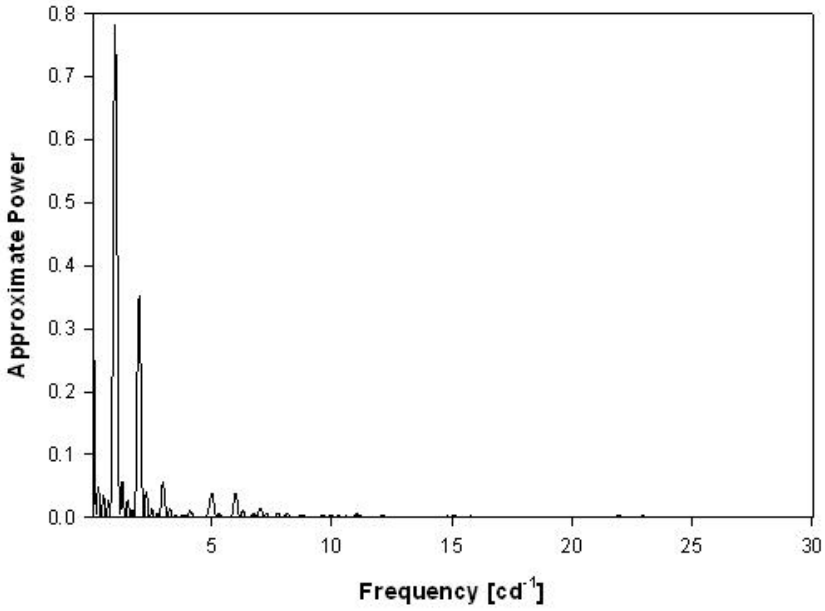

Figure 17. The spectral window function for nights 17-21 of observations.

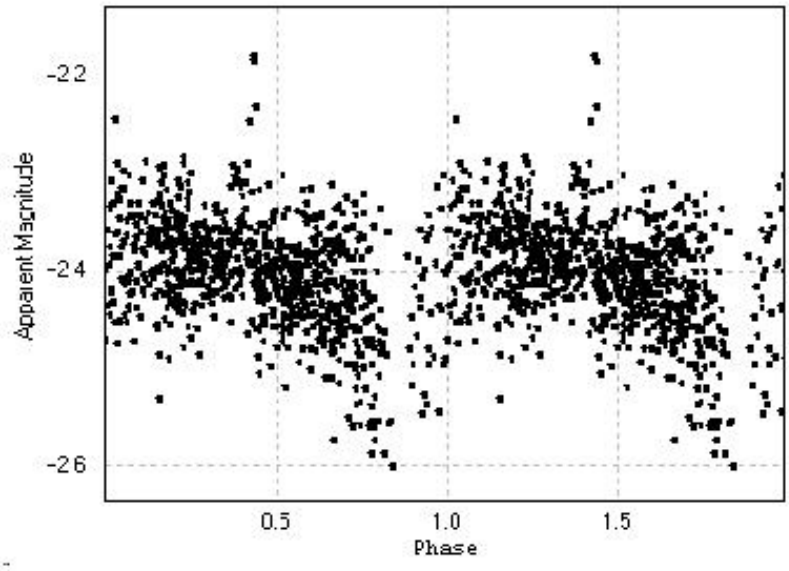

Figure 18. Phase-folded light curve over the prominent signal in Figure 16 of $F_1 = 3.039$ cycles/day (7.897 h).

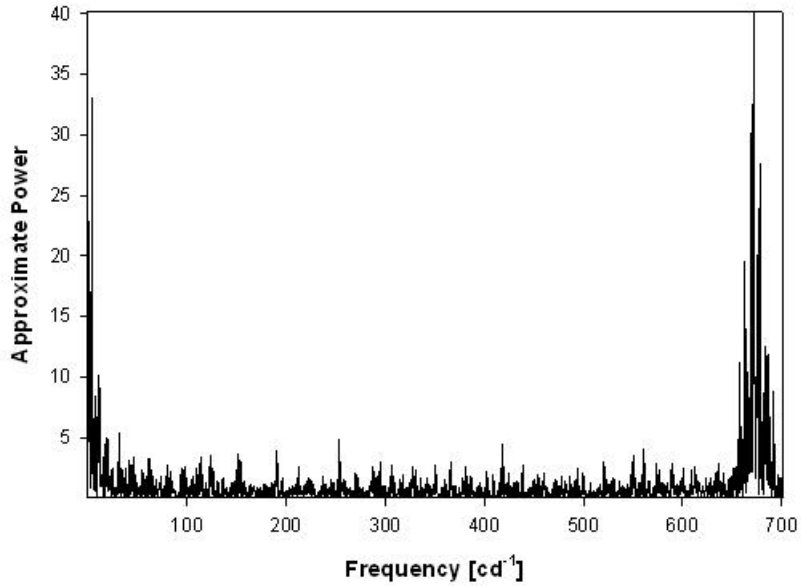

Figure 19. The full L-S periodogram for nights 17-21 of observations out to the Nyquist frequency. Note the lack of any strong high-frequency signals.

4. Nights 35-38

The fourth section spans nights 35-38, or 2012 September 13-17. The only prominent periodicity is $F_1 = 6.8941 \pm 0.0998$ cycles/day, corresponding to a period of 3.4812 h, as well as the standard 1 cycle/day aliases. The fact that this is the only signal is rather perplexing because there is no comparable signal arising within the error in the periodograms for the other sections (Figures 7, 11, 16, and 25). This value is about half of the lower limit of 6.2 cycles/day by Casares et al. (2012) obtained by spectroscopic radial velocity studies of the Hα emission from the companion. It is a definite signal since it does not coincide with identical frequencies in the SWF in Figure 21. Unfortunately, we do not have a good reason as to why the proposed orbital period of 7.897 h is absent in this periodogram. It may be possible that since the rebrightening occurred a mere 14 days before, there was still a residual luminosity that masked any shorter variability though further study is required to be certain. Figure 22 is the light curve folded over the prominent 6.8941 cycles/day signal and sinusoidal behavior is evident. Figure 23 is the full L-S periodogram including the Nyquist frequency of 340 cycles/day. There is no distinct quasi-periodic behavior evident in this periodogram.

In order to search for any periodicities that were not evident in the original periodogram analysis in Figure 20, we subtracted the prominent signal of $F_1 = 6.8941$ cycles/day from the observations and began a new periodogram analysis on the residual data. If a new signal appears in the residual periodogram, then the system may contain multiple periodicities such as the disk's precessional period, orbital period, and superhump period. This

method is called prewhitening and is very useful for finding "hidden" signals in the data. Figure 24 shows the prewhitened periodogram with the 6.8941 cycles/day signal cut out and very closely resembles the regular periodogram for nights 39-41 seen in Figure 25. However, upon closer comparison of the two periodograms, we notice that the four prominent signals of the prewhitened periodogram in Figure 24 all reside $\leq$30 cycles/day, whereas the four prominent signals of the regular periodogram in Figure 25 are less spread out and reside $\leq$25 cycles/day. One possibility for this is that if the data from nights 35-38 were still experiencing lingering effects from the recent rebrightening, which would result in a higher disk viscosity and luminosity, the movement of gas throughout the disk would have been hindered. Thus the gas would move slower and result in lower-frequency signals. So as the disk became less viscous and more transparent to light, the frequency of the observed periodicities would decrease.

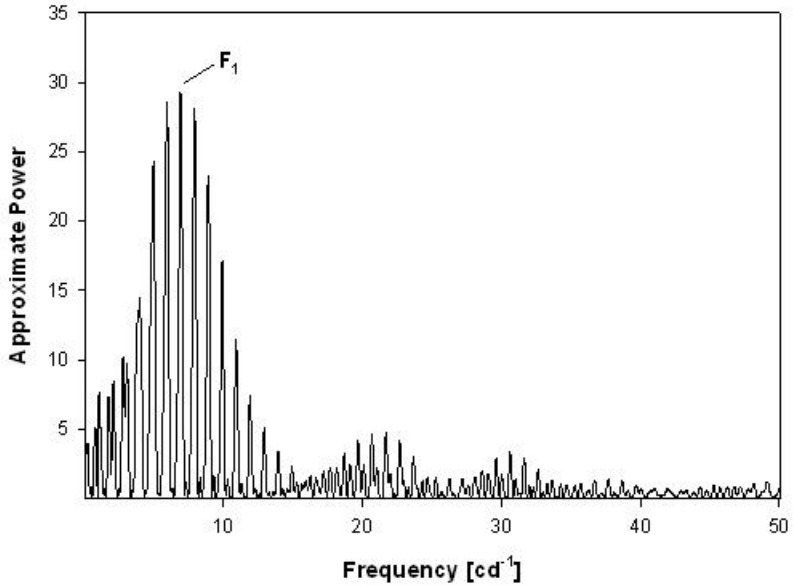

Figure 20. The L-S periodogram for nights 35-38 of observations.

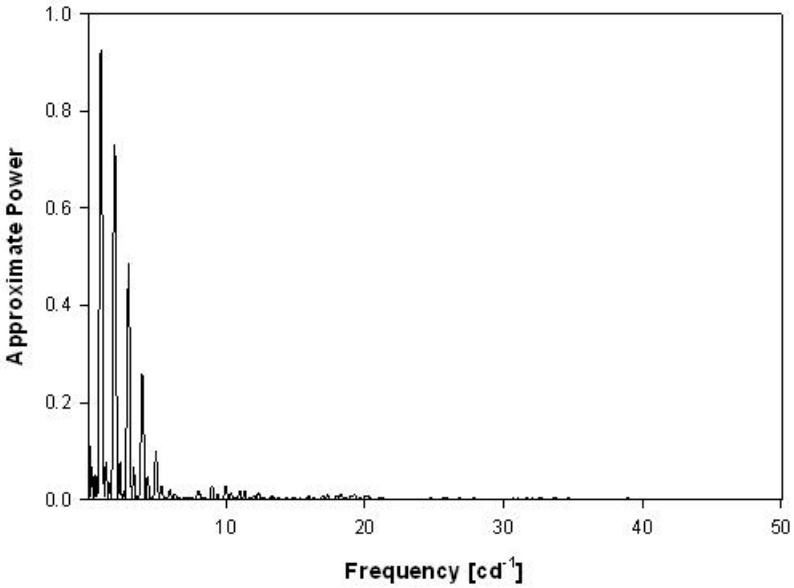

Figure 21. The spectral window function for nights 35-38 of observations.

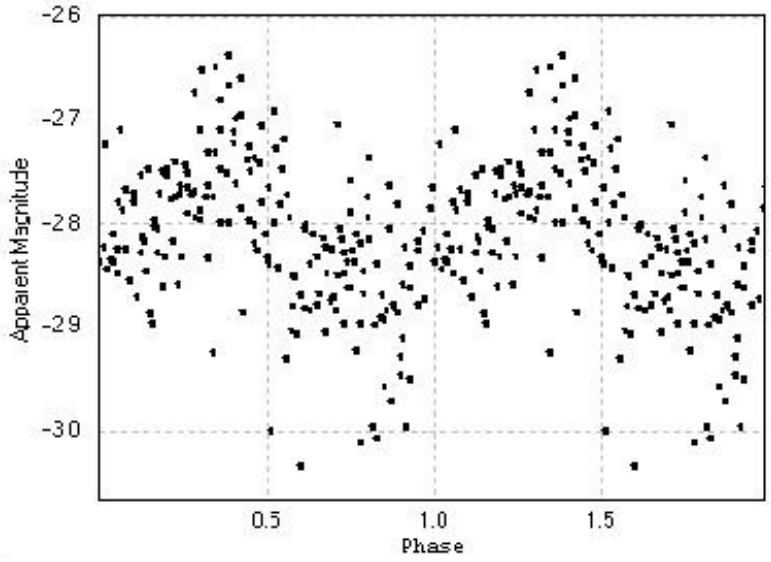

Figure 22. Phase-folded light curve over the most prominent 6.8941 cycles/day (3.4812 h) signal revealing sinusoidal behavior.

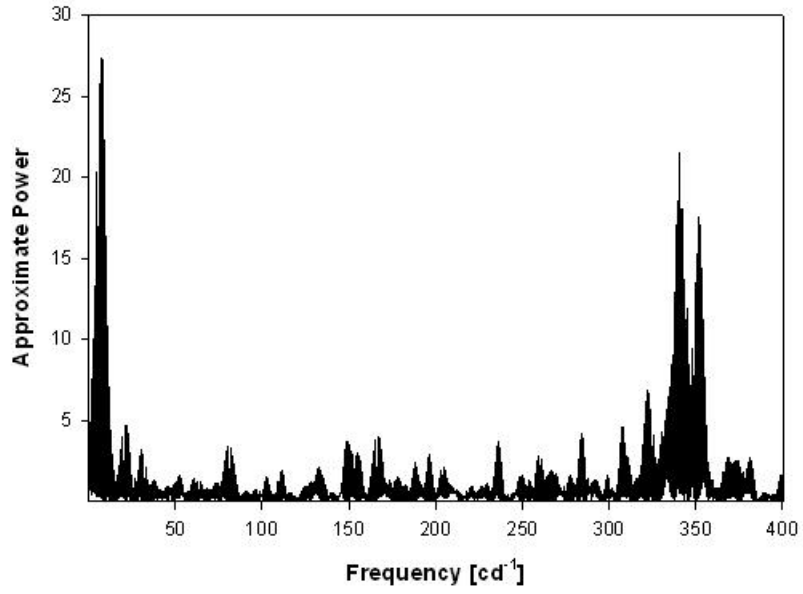

Figure 23. The full L-S periodogram for nights 35-38 including the Nyquist frequency at ∼340 cycles/day. Note the general lack of periodicities throughout the range of frequencies.

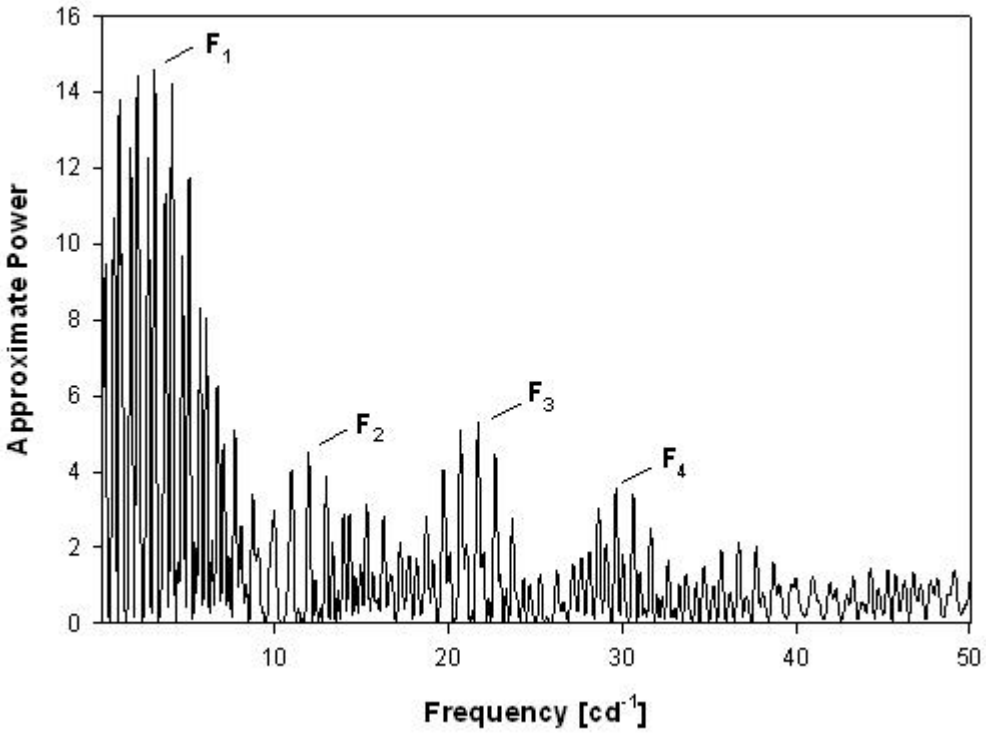

Figure 24. The prewhitened L-S periodogram for nights 35-38. Several periodicities are revealed in the residuals that resemble those found in the periodogram for nights 39-41 as seen in Figure 25.

5. Nights 39-41

The fifth and final section of consecutive observations are nights 39-41, or 2012 September 18-21. Figure 25 is the L-S periodogram and shows four distinct signals at $F_1 = 4.0605 \pm 0.0499$ cycles/day (5.9106 h), $F_2 = 11.0188 \pm 0.0014$ cycles/day (2.1781 h), $F_3 = 18.1766 \pm 0.0048$ cycles/day (1.3204 h), and $F_4 = 25.0101 \pm 0.0024$ cycles/day (57.57 min). We can see that none of these signals coincide with the signals in the spectral window function seen in Figure 26. The signals at $\sim$4 and $\sim$11 cycles/day are present in this periodogram just as they were in the periodogram for night 12-16, nights 17-21 and the prewhitened periodogram for nights 35-38. The persistence of these signals in the data spanning several months of observations is a very convincing case for them being true periodicities in Swift J1910.

Figure 27 is the full L-S periodogram including the Nyquist frequency $\sim$350 cycles/day. There is a quasi-periodicity candidate at 110.087 cycles/day, corresponding to a duration of 13.08 min. Figure 28 is the average power spectrum and was calculated using the method described earlier in the text. We note the prominent low-frequency signal of 5.91 h, the 1.32 h signal due to the $\sim$18 cycles/day peaks seen in Figure 27, and the quasi-periodicity candidate signal of 13.08 min. Since the method used to calculated the average power spectrum does not cut out short, aperiodic fluctuations, we believe that this signal of a 13.08 min quasi-periodicity to be real because a distinct spike in the power spectrum is present. Additionally, there is a great deal of high-frequency power, which is characteristic of increased flickering behavior that is evident in the periodogram. The signal at the far right of

Figure 28 is the Nyquist frequency.

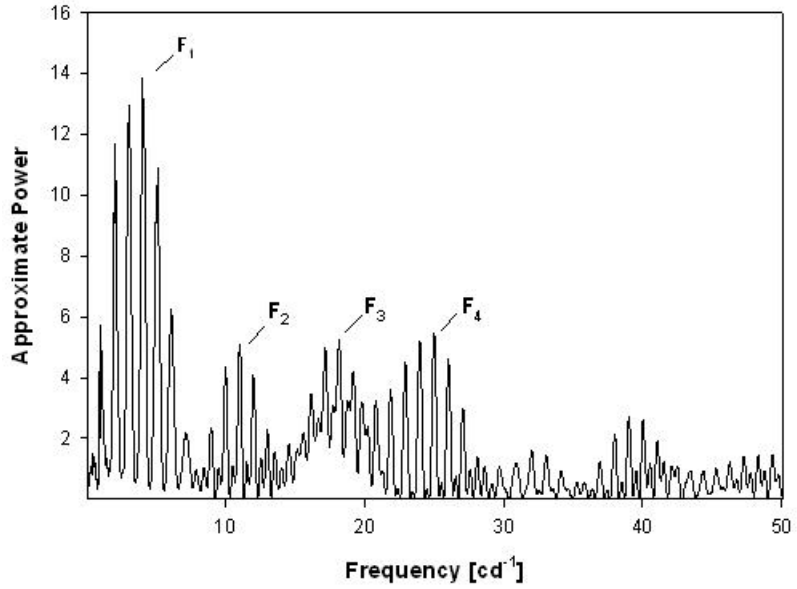

Figure 25. The L-S periodogram for nights 39-41 of observations.

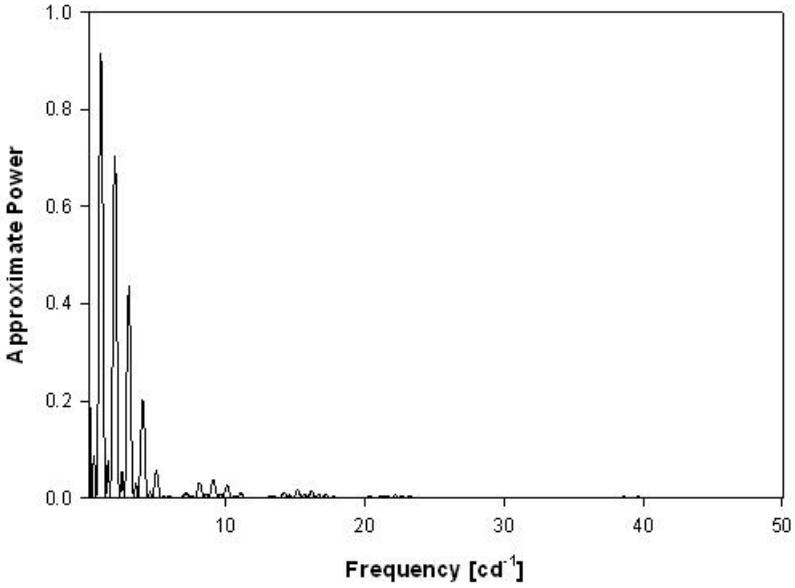

Figure 26. The spectral window function for nights 39-41 of observations.

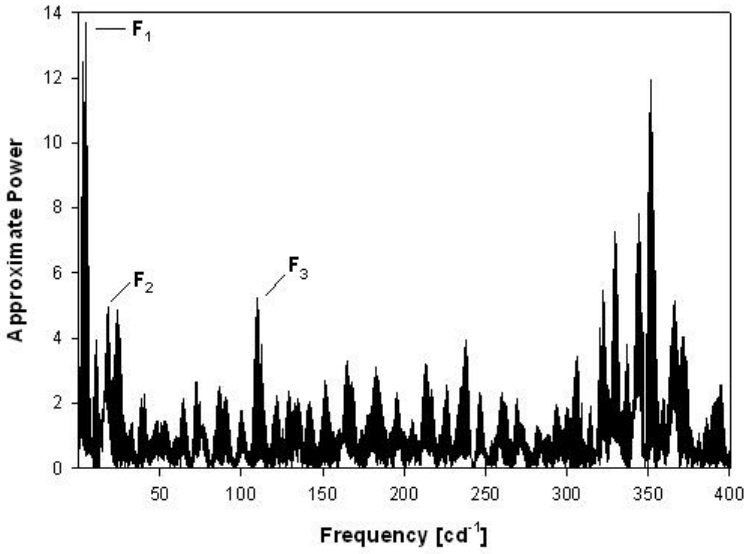

Figure 27. The full L-S periodogram of nights 39-41 including the Nyquist frequency of ∼350 cycles/day. There is strong flickering behavior as well as several quasi-periodicity candidates.

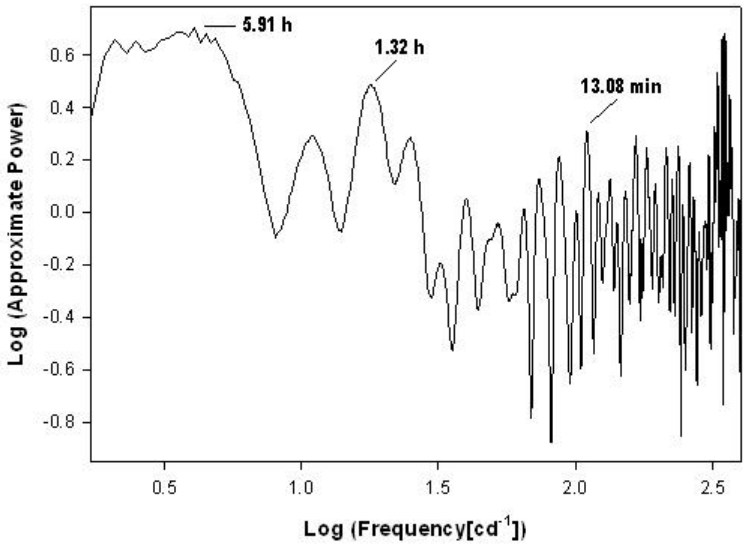

Figure 28. The average power spectrum for nights 39-41 of observations showing a great deal of high-frequency power with several quasi-periodicity candidates.

Nights 1-11		Nights 12-16		Nights 17-21		Nights 35-38		Nights 39-41	
Frequency	Error	Frequency	Error	Frequency	Error	Frequency	Error	Frequency	Error
0.064	0.012	2.9565	0.0999	3.039	0.060	6.8941	0.0998	4.0605	0.0499
0.942	0.001	10.7472	0.0038	10.749	0.007	-	-	11.0188	0.0014
1.0715	0.0017	-	-	11.7665	0.0074	-	-	18.1766	0.0048
2.059	0.002	-	-	-	-	-	-	25.0101	0.0024

Table 3. Prominent frequencies and errors for all five observing sections. All frequency values are in units of cycles/day.

Superhumps

Superhumps are a phenomenon in many closely-orbiting binary star systems. As discussed in Chapter 6 of Hellier (2001), nodal, or negative, superhumps refer to waves in the disk that are perpendicular to the disk plane and apsidal, or positive, superhumps refer to the disk becoming elongated producing waves that precess in the plane of the disk. The precessional period P_{prec} of the disk and the orbital period P_{orb} of the system may align with one another and produce a "beating" pattern that can be seen in the light curve. If we interpret the 4.0605 cycles/day (5.91 h) signal to be the precessional period P_{prec} and the 10.7485 (2.23 h) cycles/day signal to be the orbital period P_{orb}, we predict an apsidal superhump period P_{sh} of 3.59 h (see page 77 of Hellier, 2001) using the equation

$$\frac{1}{P_{sh}} = \frac{1}{P_{orb}} - \frac{1}{P_{prec}} \tag{3}$$

This matches the value for the prominent period in the periodogram analysis of nights 35-38 seen in Figure 20. As discussed in Section 6.3 of Hellier (2001),

the superhump period reaches a maximum amplitude around the time of the peak of an outburst in a cataclysmic variable. We believe this may be applied to Swift J1910 as well and that since nights 35-38 were close to the rebrightening phase, the superhump period could very well dominate any other periodicity during this time. This is the significance of the prewhitened periodogram of Figure 24. If the proposed P_{orb} is cut out of the periodogram, then we observe the normal periodicities that are evident for multiple sections of observations.

However, the interpretation of the superhump period as 6.8941 cycles/day (3.4812 h) is refuted by the discussion of superhumps in Patterson et al. (2005). We found signals at 4.0605, 11.0188, 18.1766, and 25.0101 cycles/day in the analysis of nights 39-41. These coincide well to the "beat" progression described by Ω, P_{orb}, $2P_{orb}$ - Ω, and $3P_{orb}$ - Ω, where $\Omega = 1/P_{prec}$. Superhumps are usually several percent longer (positive) or shorter (negative) than P_{orb}. Using our values for P_{sh} and P_{orb}, we find a period excess $\epsilon =$ 0.559, where

$$\epsilon = \frac{P_{sh} - P_{orb}}{P_{orb}} \tag{4}$$

Unfortunately, there are some problems with our calculations. First, in a typical binary star system, a larger value of P_{sh} - P_{orb} implies that the compact object is much more massive than the secondary (known as the mass ratio q). We note that our values of 74.89 min for this period difference and 0.559 for the period excess are extremely large. Haswell et al. (2001) used typical q values of $\sim$0.102 for SXTs. Second, Patterson et al. (2005) gives an

empirical formula for relating the period excess to the mass ratio q as $\epsilon = 0.18q + 0.29q^2$. Solving this equation for q results in a mass ratio of $q = 1.11$. Since superhumps can only occur in binary star systems with $q \leq 0.33$ as is descibed in Whitehurst & King (1991), our mass ratio of $q = 1.11$ is physically impossible. These inconsistencies point to either we have predicted incorrect period values or there are no superhumps in the system after all. The latter conclusion is somewhat curious because the observed periodicities agreed with those obtained through Equation 3. Nonetheless, the egregious values for the period excess and mass ratio lead us to conclude that superhumps were not detected in Swift J1910.

It is entirely possible that the low-frequency ∼8 h signal in the L-S periodograms of Figures 11, 16, 22, and 25 is actually the orbital period of Swift J1910 and not the precessional period. This would be supported by observations by Casares et al. (2012). In fact, we believe this to be more likely since the period excess is so large otherwise.

B, V, and R band Photometry

We took differential photometry of Swift J1910 through Johnson-Morgan Blue (B) and Visual (V) filters, as well as a Kron-Cousins Red (R) filter. These were taken over the first five weeks of observations in addition to our regular observations. The light curves are shown in Figure 29 (B band), Figure 30 (V band), and Figure 31 (R band). We note gradual downward trends in all three light curves as expected. More specifically, the luminosity of the system in the B band in Figure 29 is about the same as that

of the V band in Figure 30. Overall, both the B and V band light curves are roughly 0.2 magnitudes brighter than the R band light curve. This is attributed to the secondary reradiating the intense X-ray irradiation from the accretion disk as short rather than long wavelength optical radiation. All three filters show quasi-periodic flickering as was evident in the regular photometry as well.

Using the comparison (C4) and check stars (C5) preferred by the British Astronomical Association Variable Star Section (BAAVSS) we were able to determine mean magnitudes for Swift J1910 of $B = 16.70$, $V = 16.00$, and $R = 15.64$. Table 1 lists the CMC 14 and 2MASS designations of V, $C4$, and $C5$ and their respective magnitudes through each filter as well as the r' band. These values are consistent with observations by Cenko et al. (2012), Britt et al. (2012), and Lloyd et al. (2012), yet slightly inconsistent with Casares et al. (2012).

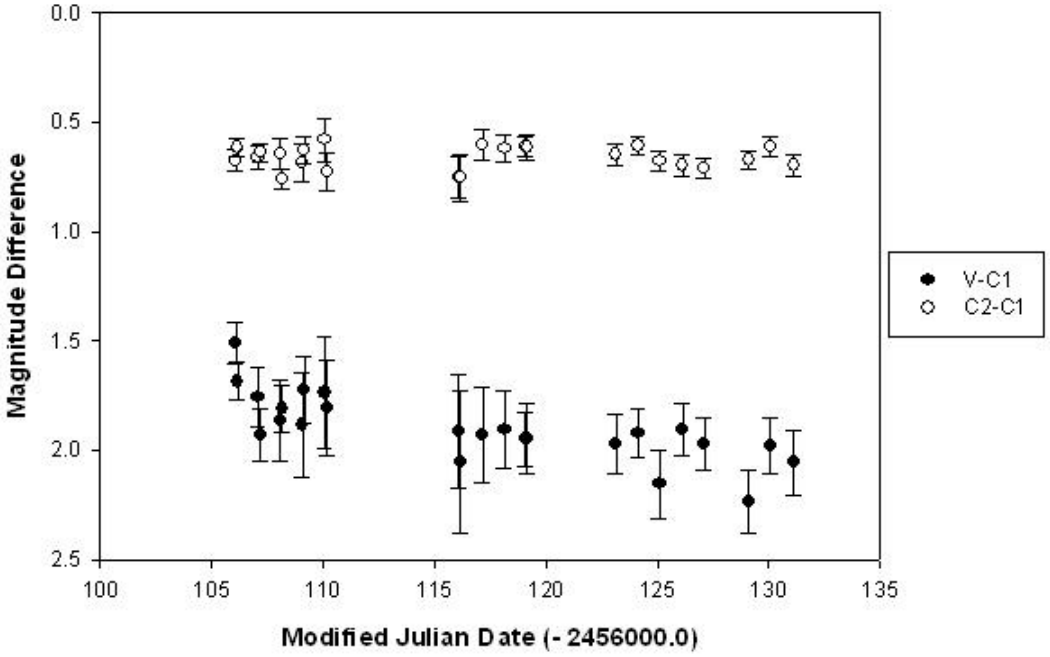

Figure 29. Differential photometric light curve through a B band filter.

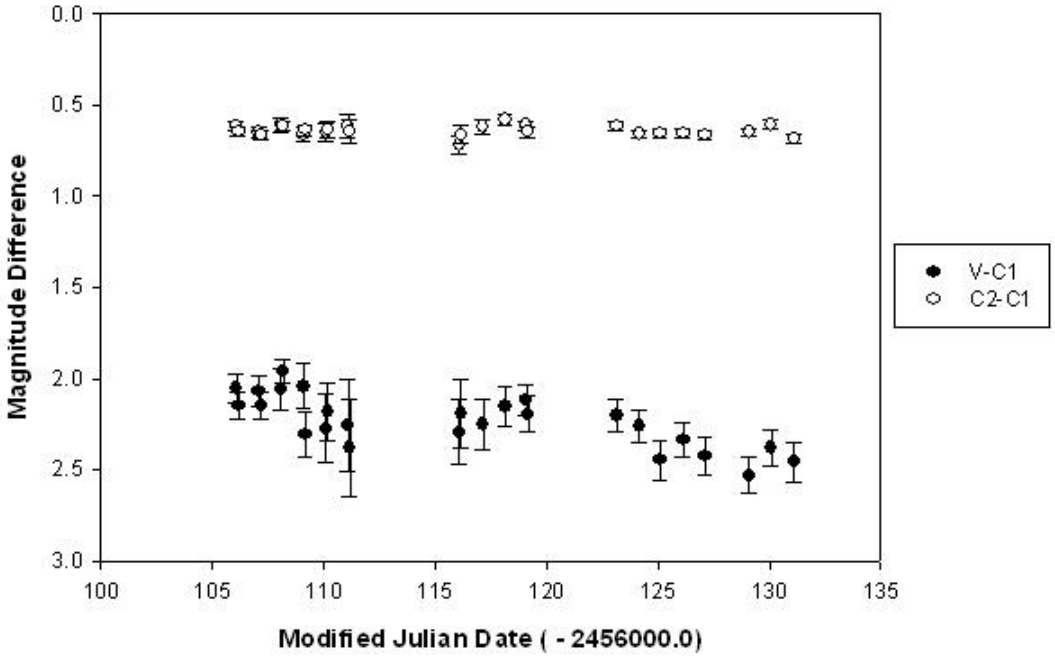

Figure 30. Differential photometric light curve through a V band filter.

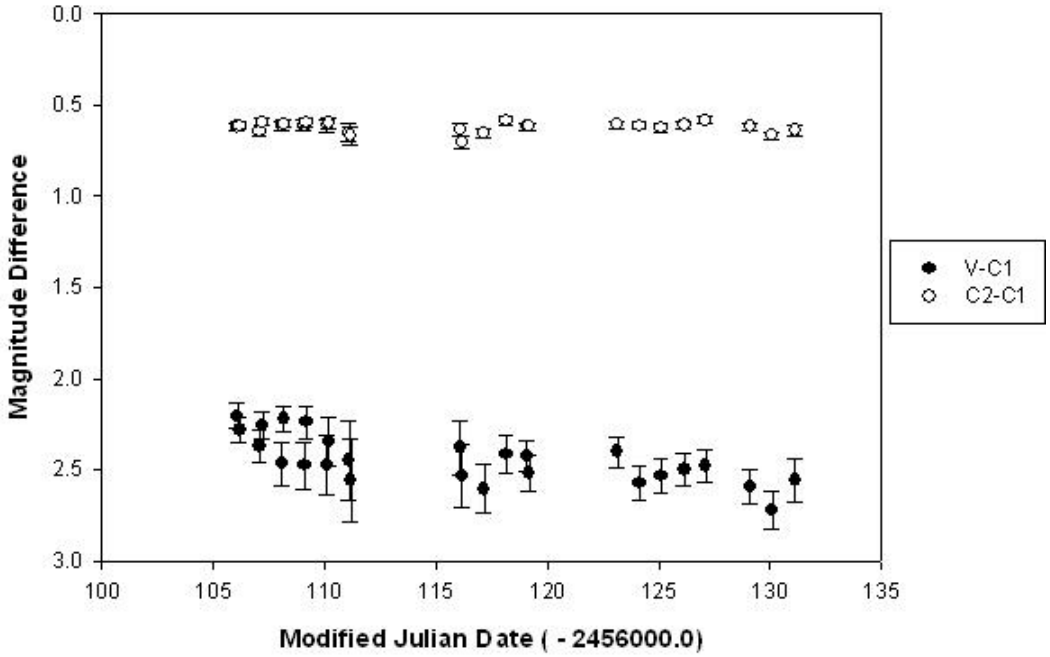

Figure 31. Differential photometric light curve through an R band filter.

CONCLUSIONS

Forty-one nights of differential photometry of the SXT/black hole candidate Swift J1910 have been presented. We found multiple periodicities in all five observing sections that spanned from 2012 June 21-22 to 2012 September 20-21. We propose two possible orbital period scenarios:

First, an orbital period of $P_{orb} = 2.233$ h (10.749 cycles/day) was proposed since it was the only periodicity found to repeat itself, within a standard deviation, in two of the five observing sections. This value for the orbital period is supported by spectroscopic radial velocity studies of the companion's Hα emission by Casares et al. (2012).

A search for superhumps was performed but no indication of which was found. The period difference of $P_{sh} - P_{orb} = 74.89$ min and the period excess of $\epsilon = 0.559$ were both greatly above the normal values. We obtained a mass ratio $q = 1.11$, which is physically impossible for binary star systems (Whitehurst & King 1991).

Swift J1910 is rife with aperiodic behavior, including a large amount of flickering. This is characteristic of LMXBs, though more evident primarily during the less luminous times of the decline (i.e. not during the rebrightening phase). Optical quasi-periodicitiess were believed to have been detected of 4.19 min during nights 12-16 and 13.08 min during nights 39-41. By comparing Figure 15 with Figure 28, we see that there is a definite increase in high-frequency power. This is believed to be because, after initial outburst, the temperature of the system cools sufficiently so that the disk becomes optically transparent, which makes it easier to observe the tiny

fluctuations of material infalling onto the compact object.

Observations through B, V, and R filters were performed. In all three filters, the aperiodic flickering behavior on the timescale of several days was still evident as well as a gradual decrease in magnitude throughout all nights of observations. Mean magnitude values of $B = 16.70$, $V = 16.00$, and $R = 15.64$ were obtained. These values make sense with the companion star reradiating the incident X-rays, resulting in an optical flux for the system containing more short wavelength light than long wavelength light. In general, these values agree with previous observations of Cenko et al. (2012), Britt et al. (2012), and Lloyd et al. (2012), however marginally disagree with those of Casares et al. (2012). Further observations in all wavelengths are encouraged and required to support or deny our conclusions.

REFERENCES

Bodaghee et al., (2012) ATel 4328.

Berry, R., Burnell, J., 2005. The Handbook of Astronomical Image Processing, Willmann-Bell, Richmond, VA.

Britt et al. (2012) ATel 4195.

Casares et al. (2012) ATel 4347.

Casares, J., X-ray Binaries and Black Hole Candidates: A Review of Optical Properties. In: *Binary Stars, Selected Topics on Observations and Physical Processes*, edited by F. C. Lázaro & M. J. Arévalo (2001) 563, 277.

Cannizzo, J. K., Wheeler, J. C., Ghosh, P., Cataclysmic Variables and Low-Mass X-ray Binaries, edited by D. Q. Lamb and J. Patterson (1985), p. 307.

Cenko, S. B., Ofek, E. O. (2012) ATel 4146.

Charles, P. A., Coe, M. J., 2006. Compact Stellar X-ray Sources, Cambridge Univ. Press, Cambridge.

Cutri, R. M., Strutskie, M. F., van Dyk, S., Beichman, C. A., Carpenter, J. M., Chester, T., Cambresy, L., Evans, T., Fowler, J., Gizis, J., Howard, E., Huchara, J., Jarrett, T., Kopan, E. L., Kirkpatrick, J. D., Light, R. M., Marsh, K. A., McCallon, H., Schneider, S., Stiening, R., Sykes, M., Weinber, M., Weinber, M., Wheaton, W.A., Wheelock, S., Zacarias, N., 2003 The IRSA 2MASS All-Sky Point Source Catalog, NASA/IPAC Infrared Science Archive. http://irsa.ipac.caltech.edy/applications/Gator/.

Haswell, C. A., King, A. R., Murray, J. R., Charles, P. A., 2001. MNRAS 321, 475.

Hellier, C., 2001. Cataclysmic Variables: How and Why They Vary, Praxis Publishing Ltd., Cornwall, U.K.

Kennea et al. (2012) ATel 4145.

Kimura et al. (2012) ATel 4198.

King et al. (2012) ATel 4295.

Kuulkers, E., 1998. NewAR 42, 1.

Lomb, N. R., 1976. ApSS 39, 447.

Lloyd et al. (2012) ATel 4246.

Mineshige, S., 1994. ApJ 431, 99.

Mineshige, S., Hirano, A., Kitamoto, S., Yamada, T. T., Fukue, J., 1994. ApJ 426, 308.

Nakahira et al. (2012) ATel 4273.

Patterson, J. et al., 2005. PASP 117, 1204.

Papadaki, C., Boffin H. M. J., Sterken C., Stanishev V., Cuypers J., Boumis P., Akras S., Alikakos J., 2006. A&A 456, 599.

Pickard, R., 2012, www.britastro.org/vss/.

Press, W. H., Teukolsky, S. A., Vetterling, W. T., Flannery, B. P., 1992. Numerical Recipes in C, 2nd ed. Cambridge Univ. Press, p. 575.

Remillard, R. A., McClintock, J. E., 2006. ARA&A 44, 49.

Scargle, J. D., 1982. ApJ 263, 835.

Seward, F. D., Charles, P. A., 2010. Exploring the X-ray Universe, 2nd ed. Cambridge Univ. Press, Cambridge.

Vanmunster, T., 2009. PERANSO software.

White, N. E., Nagase, F., Parmar, A. N., The Properties of X-ray Binaries.

In: *X-ray Binaries*, edited by W. Lewin, J. van Paradijs, & E. P. J. van den Heuvel (1995), p. 1.

Whitehurst, R., King, A., 1991. MNRAS 249, 25.